Characterization of bulk and surface properties of anion-exchange membranes in initial stages of fouling by red wine

V. Sarapulova, E. Nevakshenova, X. Nebavskaya, A. Kozmai, D. Aleshkina, G. Pourcelly, V. Nikonenko, N. Pismenskaya

Highlights (for review)

Polyphenols act an important role in membrane fouling.

Initially anthocyanins penetrate into the membrane, followed by tannins.

Colloidal aggregates fill the pores and are deposited on the surface.

In early stages, the limiting current increases and water splitting is suppressed.

All membrane properties deteriorate after long-term contact with wine.

Grafical abstract

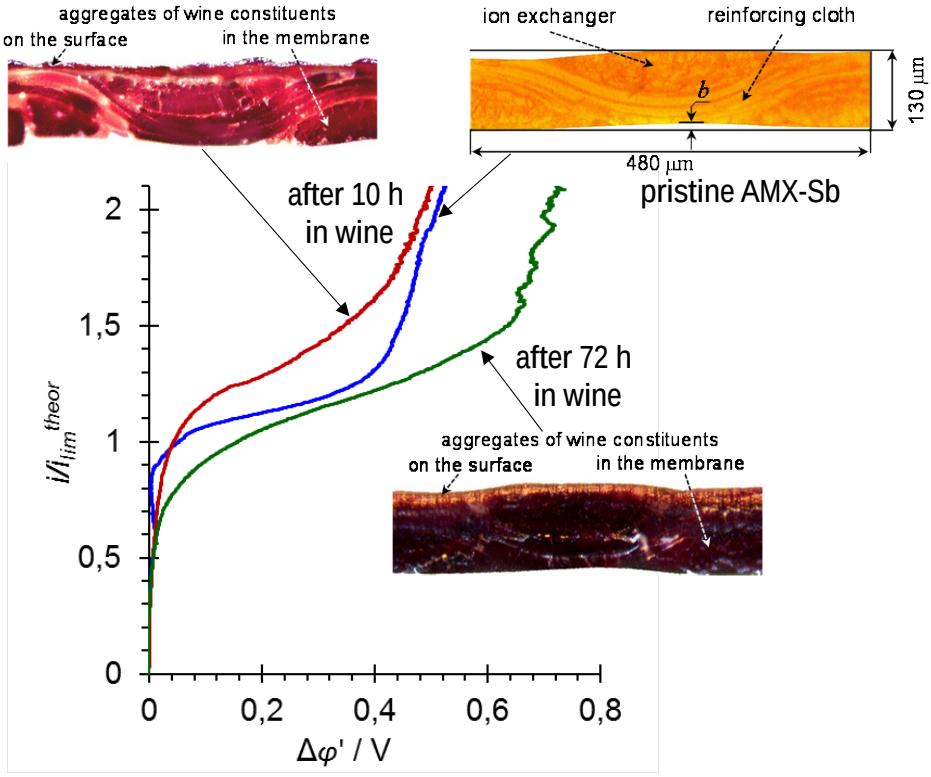

Characterization of bulk and surface properties of anion-exchange membranes in initial stages of fouling by red wine

V. Sarapulova[a], E. Nevakshenova[a], X. Nebavskaya[a], A. Kozmai[a], D. Aleshkina[a], G. Pourcelly[b], V. Nikonenko[a1], N. Pismenskaya[a]

[a] Membrane Institute, Kuban State University, 149 Stavropolskaya Street, 350040 Krasnodar, Russia

[b] Institut Europeen des Membranes, Universite de Montpellier 2, ENSCM, CNRS, CC047, Place Eugene Bataillon, 34095 Montpellier Cedex 5, France

Abstract

Electrodialysis finds broader use in reagent-free pH correction and tartrate stabilization of wines. The efficiency of these processes strongly depends on longevity of employed anion-exchange membranes. We report a comprehensive study of bulk and surface properties of a homogeneous Neosepta AMX-Sb and a heterogeneous MA-41P anion-exchange membranes after its contact with a red wine for 3, 10 and 72 hours. The ion-exchange capacity, conductivity, thickness, as well as surface roughness (AFM and optical microscopy), local surface and bulk pH (by color indicator), surface chemical structure (ATR FTIR), contact angle and surface charge are measured. In addition, the AMX-Sb membrane is characterized by voltammetry and pH-metry. It is found that polyphenols act un important role in membrane fouling. Initially, it is relatively small and mobile anthocyanins, which penetrate inside the membrane; then they are followed by larger and slower tannins and/or anthocyanin-tannin complexes. Polyphenols together with polysaccharides and other wine constituents form colloidal aggregates, which fill the membrane pores and are deposited by islets on the surface as a foulant layer. The appearance of this layer increases hydrophilicity of the surface while reducing its charge. The membrane conductivity decreases with increasing the duration of membrane contact with wine. However, the effect of this contact on the limiting current density, i_{lim}, overlimiting transfer and water splitting is unexpected. In early stages of fouling, i_{lim} of the AMX-Sb membrane increases and water splitting is found suppressed, electroconvection is essentially enhanced. The latter should be due to the isle-type structure of the foulant layer: surface electrical heterogeneity promotes electroconvection. However, the contact of the membrane with wine for several tens of hours results in formation of all-over foulant layer stimulating water splitting and reducing electroconvection.

[1] Corresponding author: v_nikonenko@mail.ru, nikon@chem.kubsu.ru (V.V. Nikonenko).

Keywords: Anion exchange membrane, fouling, wine, voltammetry, contact angle, surface charge, surface morphology, electrical resistance, water splitting, electroconvection

1. Introduction

Winemaking is multi-tonnage production, whose efficiency is rapidly progressing due to introduction of membrane technologies **[1,2]**. Membrane processes play an important role in improvement of wine quality: pH correction, dealcoholization, clarification and stabilization of wine. They gradually replace the traditional methods in the wine industry **[1,3,4]**. First, the use of membrane processes allows decreasing the production costs by transition to continuous, controlled and automated techniques, as well as by the reduction of energy consumption and wine losses. Second, the membrane technologies are more environmentally friendly, since they do not require the addition of chemicals to wine; they also reduce the problem of utilization of wastes **[5]**.

The greatest progress is achieved in the field of clarification and stabilization of wine by micro- and nanofiltration (MF and NF) **[6,7]**. In this field, “stability” denotes the lack of any adverse physical, chemical or organoleptic changes during some determined period of wine storage **[8]**. Such adverse changes include **[8,9]** the darkening or other changes in color, appearance of undesirable odours and tastes, turbidity and precipitation. The main components of such sediments are crystals of hydrotartrates of potassium and calcium.

Tartrate stability of wines can be successfully achieved via electrodialysis (ED) **[1,10]**. The advantage of this method is decrease of losses of wine and valuable components (catechins, anthocyanins and leucoanthocyanins) compared with cold stabilization and ultrafiltration **[11,12]**. Adaptation of ED to stabilization of wine and grape juice is being developed since 1970s **[13,14]**, and the industrial applications of this method have appeared in 1990s **[15,16]**. Wine circulates through the desalination compartments of an electrodialyzer while pure water, which intakes the ions to be removed, circulates through the concentration compartments. The desalination degree, which is controlled by wine conductance, is usually 15 - 20% for young, 20 - 30% for dessert and 5 - 15% for mature wines **[17,18]**. Use of electrodialysis with bipolar membranes allows conducting the tartrate stabilization with simultaneous pH correction of wines and fruit juices **[1,19]**.

Another rapidly developing fields for ED application in food and beverages industry are treatment of wastewaters, creation of water recycle systems **[20,21]**, as well as extraction of antioxidants (such as anthocyanins, proanthocyanidins and ellagitannins) from the winery wastes or increase of their concentration in fruit juices **[22,23]**. The problem of membrane fouling is

crucial in these applications. According to Mikhaylin and Bazinet **[24]**, for the membrane processes in food industry, the costs of membrane regeneration and replacement amount to 20 – 30% (pressure driven processes) to 40 – 50% (electrically driven processes) of the total costs. Hence, the control of fouling and the development of methods for its prevention play a very important role in successful exploitation of membrane modules in food and beverage industry. To solve this problem, a good understanding of mechanisms of this phenomenon is required.

Wine is a very complicated medium, which contains more than 600 components **[25]**, among them there are polyphenols (anthocyanins, tannins, etc.), polysaccharides including pectins, amino acids and proteins. Interactions between wine components are very complicated. However, colloidal interactions involving polyphenols are highlighted in literature as playing a crucial role in wine stability, clarification process and taste **[26]**, as well as in membrane fouling **[27, 28, 29, 30]**.

Interactions between wine components result in formation of different types of species, which can be classified as follows: solute molecules as ions, organic acids and sugars (<1 nm), molecules with colloidal behavior as polyphenols, polysaccharides and proteins (between 1 nm and 1 μm) and particles as microorganisms, tartaric crystals and organic precipitates (>1 μm) **[31]**. A number of studies were carried out in order to identify the species responsible for membrane fouling and the mechanism of fouling.

Membrane fouling in pressure driven processes is studied **[27,32,33,34,35,36,37]** in more details than that occurring in electrodialysis. It is shown that the protein molecules participate in intermolecular interactions with each other and in hydrophobic interactions with the membrane material **[38]**. At pH values between 3 and 3.8, typical for wine, hydroxyl functional groups of polysaccharides act as Lewis and Brønsted-Lowry bases. They serve as donors of electron pairs and acceptors of protons **[33]**, and this particular property mainly determines the interactions between the polysaccharides and membranes. Polyphenols are amphiphilic molecules with hydrophobic aromatic rings and hydrophilic phenolic hydroxyl groups. These substances play crucial role in membrane fouling not only in winemaking but also in production of other drinks (juices and beers) **[34,39]**. The aggregates of polyphenols and polysaccharides present in red wine have a strong contribution to adsorptive fouling, the interaction between polyphenols and the membrane surface is the main factor governing the fouling **[27]**. An important role is due to the π-π (stacking) interactions **[27]** between phenol rings of polyphenols and aromatic groups (e.g. styrene) of membrane matrix. Electrostatic **[27,35,40]** intermolecular and foulant-membrane material interactions are also possible. Colloidal state of organic molecules formed due to the interactions between polyphenols,

polysaccharides, amino acids and proteins is supported by weak van der Waals attraction forces and electrostatic repulsion forces **[35,41]**. The fouling leads to a significant increase in hydraulic resistance and to a decrease in productive capacity of UF and MF modules **[27]**. The reduction of membrane permeability caused by fouling can occur as blockage of UF and MF membrane pores by colloidal particles **[42,43]**. The majority of organic substances mentioned above are nutrient for microbes, hence the organic fouling is frequently accompanied by biofouling **[24,36,44]**. It should be noted that some microorganisms can be adsorbed at membrane surface as early as during the first hours of operation of membrane modules **[45]**. The source of microbial contamination can be piping, storage tanks, pretreatment systems **[46]**, where microorganisms such as those responsible for brewing **[47]** found their habitat.

As for the fouling of ion-exchange membranes, the majority of studies focuses on the interactions of ion-exchange membranes and proteins or amino acids **[24,48,49,50]**. It is found that the change in pH of treated solutions enhances fouling **[49,51]**, when the amino acids and peptides gain the charge opposite to that of the fixed groups of membranes. If the foulants are aromatic, then an AEM, which possesses an aliphatic matrix, is fouled weaker than a membrane with an aromatic matrix **[52,53]**.

Audinos **[54]** proposed the hypothesis that the most probable cause for the loss of performance of ED apparatuses and the growth in energy consumption in the tartrate stabilization of wine is the fouling of membrane stack with polyphenols. However, the details of this process, the type of interactions and the kinetics of fouling were not considered. The aging of IEMs during their long-term use in ED of food solutions is studied in Refs. **[30,55,56,57]**. It is found that in the case of cation-exchange membrane (CEMs), the use of membranes causes a decrease of their ion-exchange capacity, water uptake, electrical conductivity and thickness, while the mechanical strength changes insignificantly. In the case of AEM (which possesses the same aromatic matrix), the membrane thickness and water uptake increase, while the ion-exchange capacity and electrical conductivity change slightly and the mechanical strength decreases dramatically. The hydrophilicity of CEMs decreases while the hydrophilicity of AEMs increases. It is suggested **[30,55]** that one of the reasons for the difference in behavior of CEMs and AEMs is the formation of organic colloidal particles inside the membrane pores; these particles interact differently with the fixed groups and matrix of CEMs and AEMs. As far as we know, the effect of fouling on the electrochemical behavior of the membranes, which contacted with wine, was not studied yet.

In this paper, a comprehensive study of the kinetics of anion exchange membranes fouling in initial stages caused by their contact with red wine is presented for the first time.

Different methods of surface visualization (AFM and optical microscopy), analysis of the chemical structure (ATR FTIR spectroscopy) as well as membrane physico-chemical (ion-exchange capacity, water content, thickness) and electrochemical (voltammetry, electrokinetic measurements, pH-metry) characterization are applied. Initial stages of fouling are investigated and a possible overall scenario of this process is suggested. Besides of the description of membrane performance degradation, we show that in early stages of fouling, an improvement of certain membrane properties occurs: water splitting is partially suppressed and electroconvection is increased.

2. Experimental

2.1. Membranes and solutions

A homogeneous AMX-Sb anion-exchange membrane (Astom, Japan) is selected for this study, as it is frequently used in ED treatment of liquids in food industry (processing of whey, wine, juices, etc.). This membrane is manufactured by the paste method **[58]**. The ion-exchange matrix of AMX-Sb consists of a copolymer of styrene and divinylbenzene. The fixed groups are mainly quaternary ammonium bases **[58]**. The membrane contains also an inert filler: the granules of polyvinyl chloride, whose diameter is about to 60 nm**.** Along with the AMX-Sb membrane, some experiments are made with a heterogeneous anion-exchange MA-41P membrane (Schekinoazot, Russia). MA-41P is a heterogeneous macroporous membrane produced by hot pressing of powdered AV-17-2P anion exchange macroporous resin and low pressure polyethylene acting as an inert binder. The capron net serves as a reinforcing cloth. The AV-17-2P resin is a regularly crosslinked copolymer of divynilbenzene and styrene with fixed quaternary ammonium bases as functional groups **[59]**. About 80% of the MA-41P membrane surface is covered with polyethylene. The resin particles, which protrude through the polyethylene, provide ion conduction of the membrane. The main characteristics of this membrane are presented in **Table 1.**

Table 1. Main properties of AMX-Sb and MA-41P membranes

Property	Value	
	AMX-Sb	MA-41P
Type	homogeneous, strong base [a]	heterogeneous, strong base[d]
Thickness in 0.02 M NaCl solution, μm	130 ± 10 [b]	530 ± 10 [b]

Conductivity in 0.02 M NaCl solution, S m^{-1}	0.28 ± 0.02 [b]	0.41 ± 0.02 [b]
Ion exchange capacity, meq g^{-1} (swollen membrane)	1.30 ± 0.05 [b,c]	1.25 ± 0.05 [b,d]
Water content, g H_2O (g dry membrane)$^{-1}$	0.20 ± 0.05 [b]	0.50 ± 0.05 [b]
Membrane density, g cm^{-3}	1.10 [c]	1.16[d]

[a] Manufacturer's data **[58]**.
[b] Our measurements.
[c] **[60]**.
[d] **[61]**

Distilled water (the electrical conductivity was 0.5 μS cm^{-1} at 25°C, pH = 5.5), solid NaCl (analytical grade, OJSC Vekton) and red dry Mourvèdre/Syrah/Grenache wine (pH = 3.5) were used in the experiments.

Before the study, AMX-Sb and MA-41P membranes underwent standard salt pretreatment **[62]** and then were equilibrated with a 0.02 M NaCl solution. Then each membrane sheet was divided into several samples. One sample was left pristine for the comparison, while the others were fouled by red wine in a two-chamber dialysis flow cell. The red wine circulated through one of the chambers for a certain time, and a 0.02 M NaCl solution (pH 6.0 ± 0.5), through the other; no current was applied. Thus, the fouling of the membrane occurred only from one of its sides. The symbol related to the samples fouled with wine is indicated with subscript "*w*", the time of contact in hours is marked with a number in the subscript. Thus, "AMX-Sb_{w10}" denotes the sample, which was in contact with wine during 10 hours; "AMX-Sb_{w72}" relates to the sample, which was in contact with wine during 72 hours.

2.2. Methods

The water contact angle of surface of a swollen membrane sample was determined as a function of time of its contact with wine. The sessile drop technique according to the procedure described in **[63]** was applied. The test liquid was distilled water. The contact angles reported in this paper were registered 20 seconds after the application of a test drop.

The charge density of the surface of a swollen AEM was calculated from zeta potential, which in turn was found from tangential streaming potential measurements. We employed a laboratory-made gap cell similar to that applied in Anton Paar SurPASS 3. Note that the latter is used, in particular, for the measurements of this kind in the case of ion-exchange membranes **[64]**. The construction and distinguishing features of our set-up are described in detail by Sabbatovskii et al. **[65];** the cell was equipped with two Ag/AgCl electrodes and connected to a GW Instek multimeter. The measurements of tangential streaming potential and its use for calculation of the space charge density are presented in our earlier publication **[66]**. Two

identical rectangular AEM samples formed a slit channel with 25 mm × 2.5 mm × 70 μm dimensions (length×width×height). Prior to streaming potential measurements, the fouled membranes were stored for 24 hours in a 0.02 M NaCl solution (pH=6.7) or in a 0.02 M NaCl solution, pH of which was lowered to 3.5 ± 0.1 by addition of HCl. Soaking in a 0.02 M NaCl solution was aimed at two goals: transition of the membrane to the Cl^- form and stabilization of its properties. Auxiliary measurements have shown that the electrical conductivity of a fouled in wine membrane rapidly changes after the first hour of soaking. Then the rate of conductivity variation slows down and becomes quite low after 24 h. of soaking. However, the conductivity does not return to its value of the pristine membrane. Hence, we concluded that 24 hours are sufficient for relative stabilization of membrane properties, but are not enough for restoration of membrane properties. The use of solutions with different pH was made in order to study the response of the surface charge on the pH of the bathing solution.

The measurements of streaming potential were carried out at 20 °C using a 0.02 M NaCl (pH 6.7± 0.1) solution pumped with a linear flow rate of 40 – 70 cm s^{-1}, when the pressure drop between the channel inlet and outlet was in the range from 0.125 bar to 0.625 bar.

The visualization of surface and cross-sections of swollen AMX-Sb membranes was carried out using a SOPTOP CX40M optical microscope (China) with a set of 5x, 10x, 20x, 50x and 10x objectives and a digital eyepiece camera and another optical microscope Altami BIO-2 (Russia) with a set of 4x, 10x, 40x and 100x objectives and a digital eyepiece camera. One side of the membrane under study contacted with an anthocyanin solution (10 mg L^{-1}, pH 3.5 ± 0.1) for 10 hours or with wine (pH 3.5 ± 0.1) for 3, 10 or 72 hours in a dialysis cell, as described in Section 2.1. Each membrane was cut into four pieces before visualization. The first piece was investigated immediately while the others were soaked for an hour in a buffer solution at pH 1.7 ± 0.1 (the second piece), a buffer solution at pH 6.7 ± 0.1 (third piece) or a buffer solution at pH 9.2 ± 0.1 (the fourth piece) and then photographed.

The morphology and surface relief of the air-dry AMX-Sb_w samples were studied by the AFM method in a contactless mode (JEOL 5400 microscope, Japan, JEOL 5400 software). Different parts of the sample surface were scanned each at least 10 time. The obtained data were processed using statistical analysis.

The chemical composition of the air-dried AEM surface and air-dried wine (both **at 45 °C**) were studied by ATR-FTIR spectroscopy using the disturbed total internal reflection method with a Vertex-70 spectrometer (Bruker Optics, Germany) in the range 4500 – 450 cm^{-1}. The IR spectra were processed using OPUS ™ software.

The current-voltage characteristics, the counterion transport numbers in the

membrane samples, the difference in pH between the desalination channel outlet and inlet were measured using an ED flow cell with an Autolab PGSTAT100N potentiostat/galvanostat. The flow-through four-compartment ED cell as well as overall setup and the procedure of data registration and processing are described in detail in **[67,63]**. The central desalination compartment of the cell was formed by an AEM under investigation and an auxiliary MK-40 cation-exchange membrane, which separated the central compartment from the (platinum) cathode compartment. Another auxiliary AEM membrane (an AMX-Sb one) was placed between the AEM under study and the platinum anode. The parameters of the desalination compartment were as follows: the intermembrane distance, *h*, was 6.5 mm; the linear flow rate of the 0.02 M NaCl solution, *V*, was 0.4 cm s^{-1}; the polarized area of the membrane was 2 × 2 cm^2; pH of the solution was equal to 6.0 ±0.2. The investigations were carried out at 20 ± 1 °C.

The theoretical value of the limiting current density was calculated using the Lévêque equation obtained in the framework of the convection-diffusion model **[68]**:

$$i_{\lim}^{theor} = \frac{FDC}{h(T_{Cl} - t_{Cl})}\left[1.47\left(\frac{h^2 V}{LD}\right)^{1/3} - 0.2\right] \qquad (1)$$

where *L* is the length of the desalination channel (2 cm); *C* is the molar NaCl concentration at the channel entrance; T_{Cl} and t_{Cl} are the transport numbers of the Cl^- ion in the membrane and the solution, respectively; *D* is the diffusion coefficient of NaCl in solution at infinite dilution; *F* is the Faraday constant.

The application of Eq. (1) for the membrane system under study gives $i_{\lim}^{theor}$=2.9 mA cm^{-2}.

When comparing different membrane systems, instead of the total potential drop, $\Delta\varphi$, the reduced potential drop, $\Delta\varphi'$, is used **[69]**:

$$\Delta\varphi' = \Delta\varphi - iR_{ef} \qquad (2)$$

where the effective resistance of the membrane system at current density $i \to 0$, $R_{ef} = \partial\Delta\varphi / \partial i_{i\to 0}$ (Ohm cm^2), includes the ohmic resistance of the space (membrane + solution) between the measuring electrodes and the diffusion resistance of the enriched and depleted diffusion boundary layers (DBLs). The value of R_{ef} is found by an extrapolation using the experimental current-voltage curves (CVC). The use of $\Delta\varphi'$ allows eliminating errors associated with possible changes in the distance between the surface of the membrane and the tips of Luggin capillaries during assembly and disassembly of membrane stack. As well, this excludes the effect of changes in the membrane ohmic resistance caused by its fouling on the shape of the CVC.

The method of measurement of the ion transport numbers in IEM in the case of competition between the salt counterion and the H^+ (or OH^-) ions generated in water splitting reaction at the membrane/depleted solution interface is described in Ref. **[70]**. The method is applied in relatively dilute solutions where the transport of salt co-ion through the membrane can be neglected. The idea is in the measurement of the mass-transfer rate through the membrane under study in batch mode where an intermediate tank is used in the desalting stream. When the desalted solution is acidified with time, a NaOH solution is added into the tank in order to maintain pH=7 there. An acid is added, if the solution in the tank becomes alkaline. The mass transfer rate is found by the rate of the salt concentration decrease in the tank taking into account that the salt concentration in the tank varies due to ion transfer through IEMs in the ED cell and due to addition of alkaline (or acid). The transport number of counterion is determined from the ratio of its flux density through the membrane and the current density measured with an amperemeter.

3. Results and discussions

3.1. Characteristics of membrane surface and volume

3.1.1. Morphology and surface relief of air-dry samples

Fig. 1 shows the AFM images of air-dry samples of the pristine AMX-Sb and the AMX-Sb_{w72} sample, which was in contact with wine by one of its sides for 72 hours. The results of statistical processing of 10 topographic images obtained for each of the samples are given in **Table 2.**

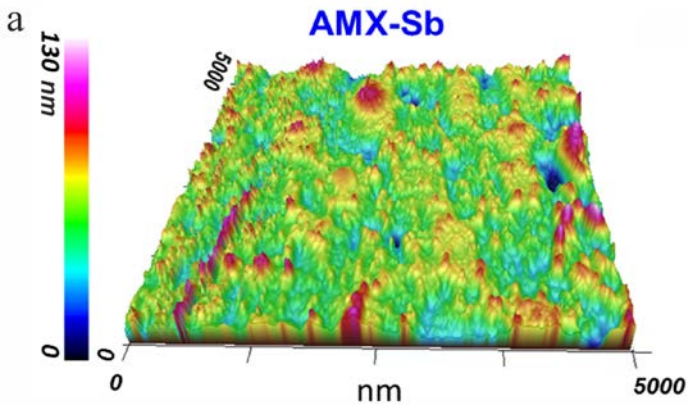

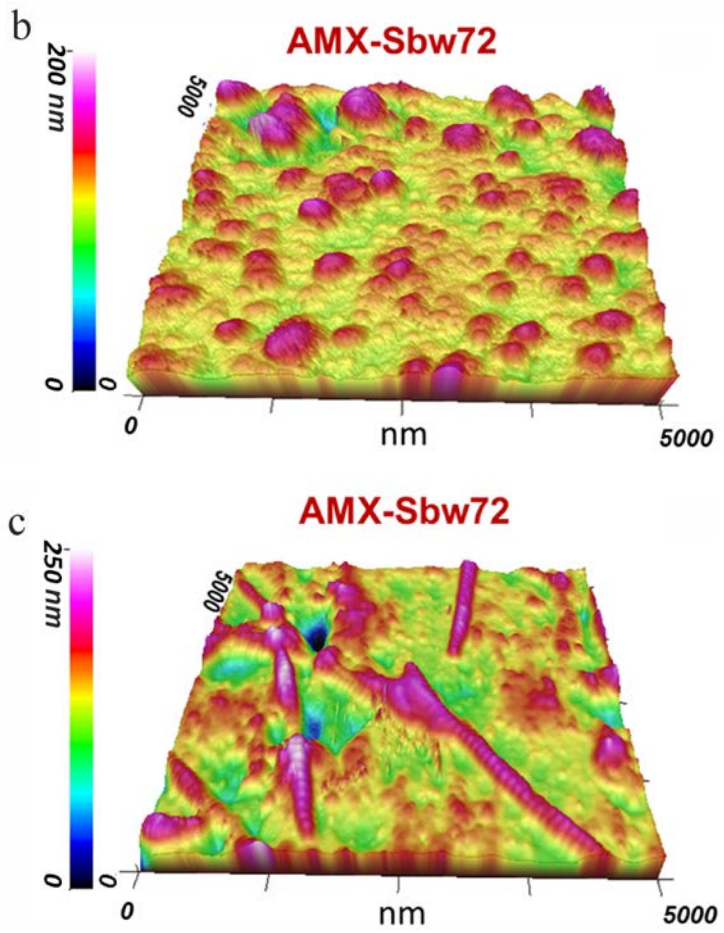

Fig. 1. AFM images of air-dried samples of AMX-Sb (a) and AMX-Sb_{w72} (b, c); the image shown in (c) reveals the presence of subjects similar to bacteria.

Table 2. Surface roughness parameters of the pristine and fouled membranes

Parameter	Membrane	
	AMX-Sb	AMX-Sb_{w72}
R_z, nm	89 ± 20	133 ± 22
S_{ratio}	1.03 ± 0.01	1.06 ± 0.01
R_q, nm	19 ± 5	27 ± 4

R_z is the ten point height of irregularities (ISO 25178-2-2014),
S_{ratio} is the roughness factor, defined as the ratio of the real surface area to the geometric area, the latter is the projection of the real surface on a plane parallel to the macroscopic visible phase boundary considered as ideally flat **[71]**,
R_q is the root mean square deviation of the assessed profile (ISO 18115-2:2013),

In the case of AMX-Sb (**Fig. 1a**), sharp peaks and valleys are randomly distributed over the area of the sample. An average width of the local protrusions is about **60** nm, which corresponds to the average linear size of the PVC granules involved in the membrane structure formation.

The local protrusions on the AMX-Sb_{w72} surface (**Fig. 1b**) have a more rounded shape. The values of all roughness parameters increase in comparison to those for the pristine membrane (**Table 2**). For example, the value of R_z, which is the average value of the absolute values of the heights of the five highest peaks and the depths of the five deepest valleys **[72]**, increases by a factor of 1.5. This change in the surface relief is similar to that observed in other studies **[73,74]** for the membranes fouled with proteins and aromatic amino acids. Some parts of the AMX-Sb_{w72} surface contain the subjects, which are similar to rod-shaped bacteria (**Fig. 1c**). The surface relief in the immediate vicinity of these subjects appears similar to that of the pristine membrane.

3.1.2. Optical microscopy of swollen samples

Fig. 2 show optical micrographs of the swollen pristine and fouled AMX-Sb membranes. The pristine AMX-Sb membrane is found reddish-orange in the pH range from 1 to 10 (**Figs. 2a and 2b**), the threads of reinforcing cloth may be seen. The size of "mesh" formed by the reinforcing cloth is (380 × 480) ± 10 μm. The valleys on the surface are observed in the areas where the threads are close to the membrane surface (**Fig. 3b**), and the protrusions are observed where the threads are distanced from the surface. It is explained by the fact that the threads obstruct swelling of the membrane material **[75]**. Thus, the surface of the swollen AMX-Sb membrane and its fouled samples is wavy; the difference between the highest and lowest points of the surface, *b*, is about 20 ± 2 μm. The parameters above characterizing the waviness of the AMX-Sb surface are close to those found in other publications **[76,66]**.

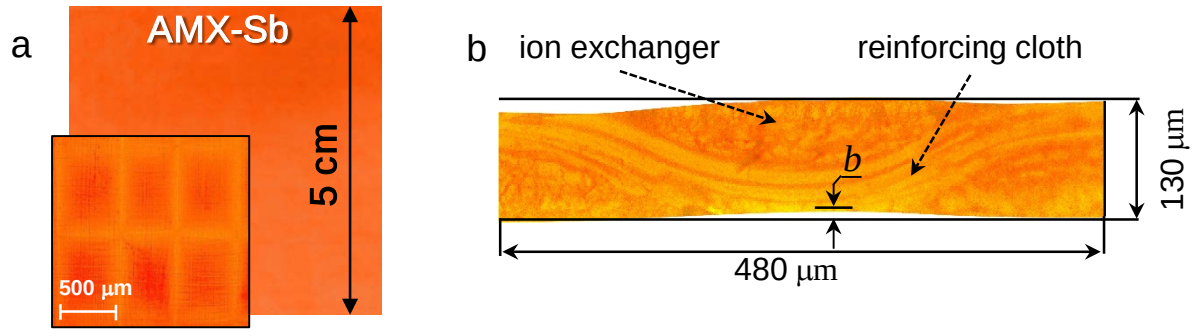

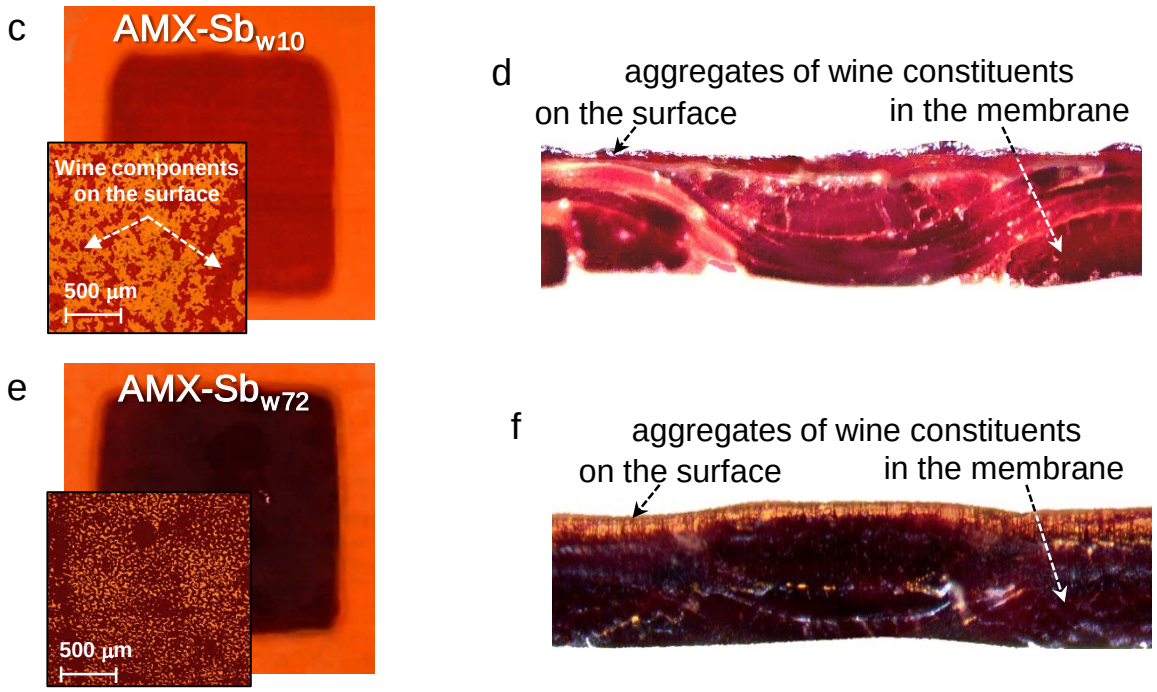

Fig. 2. Optical images of the surface (a, c, e) and cross-section (b, d, f) of the swollen AMX-Sb (a, b), AMX-Sb$_{w10}$ (c, d) and AMX-Sb$_{w72}$ (e, f) samples. In all cases the membrane face shown in the images was in contact with a solution of pH=3.5: the AMX-Sb, with an acidified 0.02 M NaCl solution for 24 h, and AMX-Sb$_{w10}$ and AMX-Sb$_{w72}$, with wine for 10 h and 72 h, respectively.

Some bulk properties of AMX-Sb and MA-41P membranes after their contact with wine are shown in **Table 3**. As for the membrane thickness, this parameter increases by 1.5 % and 5.9 % (in comparison with the pristine membranes, Table 1) in the cases of AMX-Sb and MA-41P membranes, respectively, when the time of soaking is 10 h. This increase in thickness is 3.0% (AMX-Sb$_{w72}$) and 7.2% (MA-41P$_{w72}$), when the time of soaking is 72 h (**Figs. 2b, d, f**).

Table 3. Variation of bulk properties of AMX-Sb and MA-41P membranes after their contact with wine

Membrane	Thickness, µm	Exchange capacity (swollen membrane), meq g^{-1}	Water content, g H_2O (g dry membrane)$^{-1}$	Conductivity in 0.02 M NaCl solution, S m^{-1}
MA-41P	527	1.24	0.52	0.41
MA-41P$_{w10}$	558	-	-	0.13
MA-41P$_{w72}$	565	1.18	0.53	0.06
AMX-Sb	136	1.30	0.20	0.28
AMX-Sb$_{w10}$	138	-	-	0.06
AMX-Sb$_{w72}$	140	0.77	0.27	0.03

The optic images of pristine and fouled membranes are given in **Figs. 2, 3 and 4**. The images of AMX-Sb_w (**Fig. 2**) are taken immediately after disassembling the dialysis cell (where the membrane was fouled) and rinsing the membrane with distilled water. Hence, it is presumed that the observed coloration corresponds to the pH of wine, which was 3.5. The images of fouled MA-41P membrane (**Figs. 3, 4**) are obtained after soaking the previously fouled samples in three buffer solutions with different pH values (1.68, 6.68 or 9.18) for 1 h, as described in Section 2.2.

The surface of fouled AMX-Sb_w membrane is covered with spots, which are pale ruby after the contact with wine (pH = 3.5, see **Fig. 2c**) for 10 h, and become red-brown after 72 h of the contact (**Fig. 2e**). The color of the bulk of AMX-Sb_w membrane undergoes similar changes: it is pale ruby after 10 h of contact with wine (**Fig. 2d**), and dense deep purple after 72 h of contact (**Fig. 2f**). Following the hypothesis presented above, the first color (**Fig. 2d**) can be attributed to the anthocyanins, and the second one (**Fig. 2f**), to the complexes of anthocyanins with tannins and polysaccharides **[78]**. Special side illumination of the cross-section (**Fig. 2f**) reveals a tawny colored layer, which has thickness of several micrometers and which fairly evenly covers the surface of the AMX-Sb_{w72} membrane. The way the color of this layer changes depending on the direction of illumination suggests the openwork structure of this layer and its high water content. After 10 h (**Figs. 2c and 2d**) of contact with wine, this foulant layer is seen also, however, it is not continuous, but rather island-like.

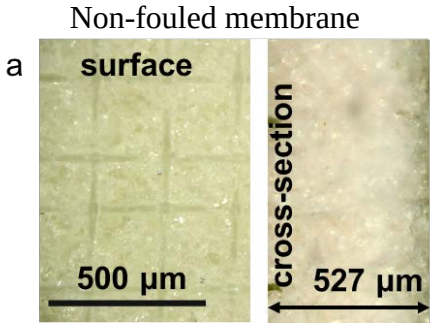

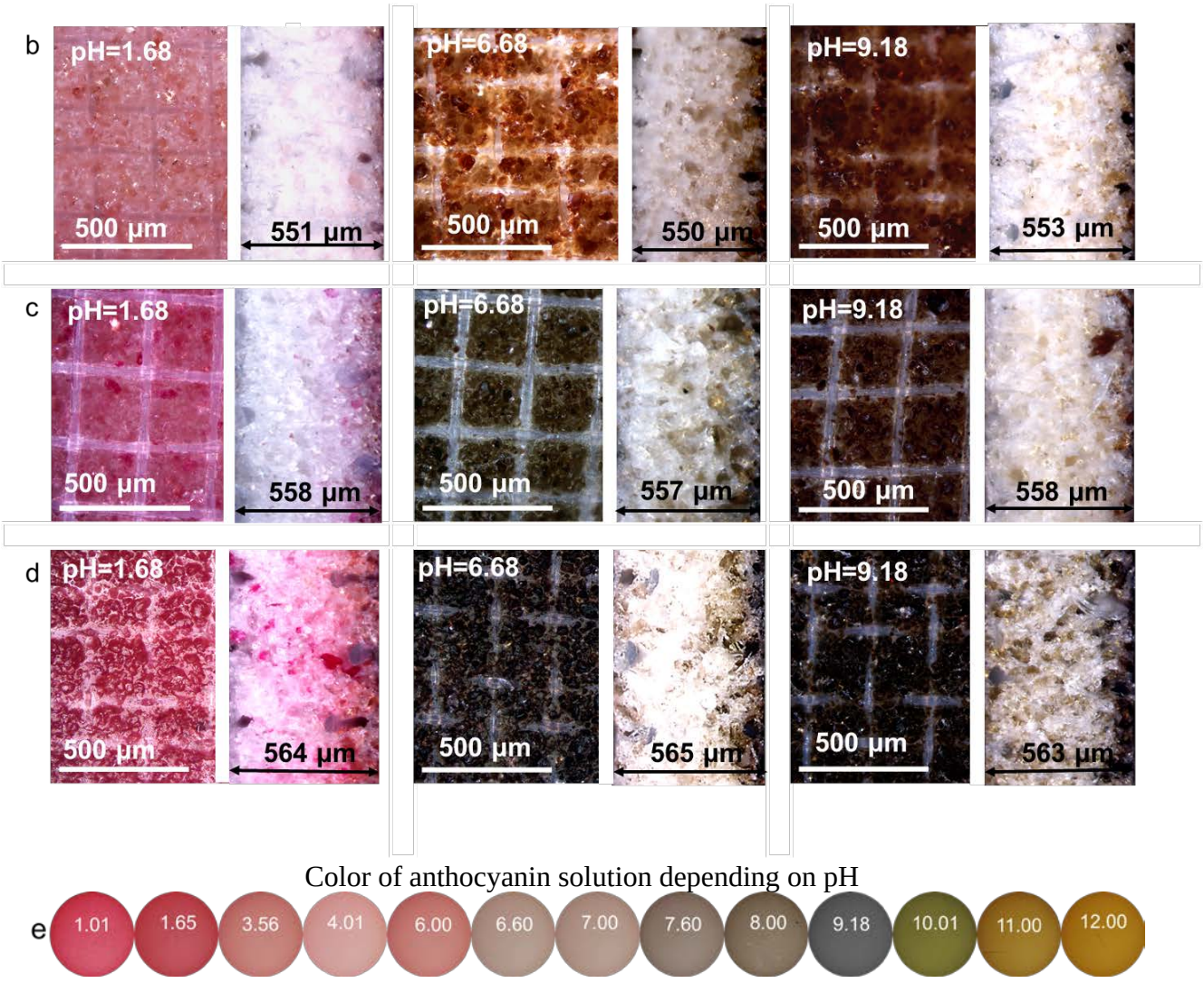

Fig. 3. Optical images of the surface and cross-section (a, b, c, d) of the swollen MA-41P membrane; (e) shows the color of an anthocyanin water solution as a function of its pH. The first line (b) shows the colors of the membrane after contact with wine for 3 h and then stored in buffer solutions with pH=1.68 or 6.68 or 9.18 for 1 h. The second (c) and third (d) lines present similar images in the cases where the membrane was contact with wine for 10 h and 72 h, respectively. The distance between the tips of the arrow in (a) corresponds to the membrane thickness.

Optical images of samples obtained at different pH values (**Figs. 3b, c, d, 4**) allow tracing the kinetics of fouling and get an idea of the composition of the foulants within the membranes and on their surface. It is important to note that in the first few hours of contact of the heterogeneous membrane with wine, the foulants are localized only on the ion-exchange particles and are nearly absent on the surface occupied by polyethylene (**Figs. 3b, c, 4 c**). Increasing the time of contact with wine leads to the expansion of the spots of the foulant around

the ion-exchange particles (**Figs. 3d, 4d**). The formation of such an island-like structure is apparently facilitated by electrostatic interactions of the wine components with the fixed groups of ion-exchange material, as well as by π-π interactions of the aromatic fragments of membrane matrix with polyphenols. Most likely, similar processes (i.e. preferential adsorption of wine components on the ion exchange material) also occur in the case of the homogeneous AMX-Sb membrane, which is a composite of an aromatic ion-exchange polymer and an aliphatic binder (polyvinyl chloride). Then this explains the island-like formation of foulant aggregates, which is observed in the first few hours of contact with wine on the surface of both homogeneous (**Fig. 2c**), and heterogeneous (**Figs. 3b, c, 4c**) membranes.

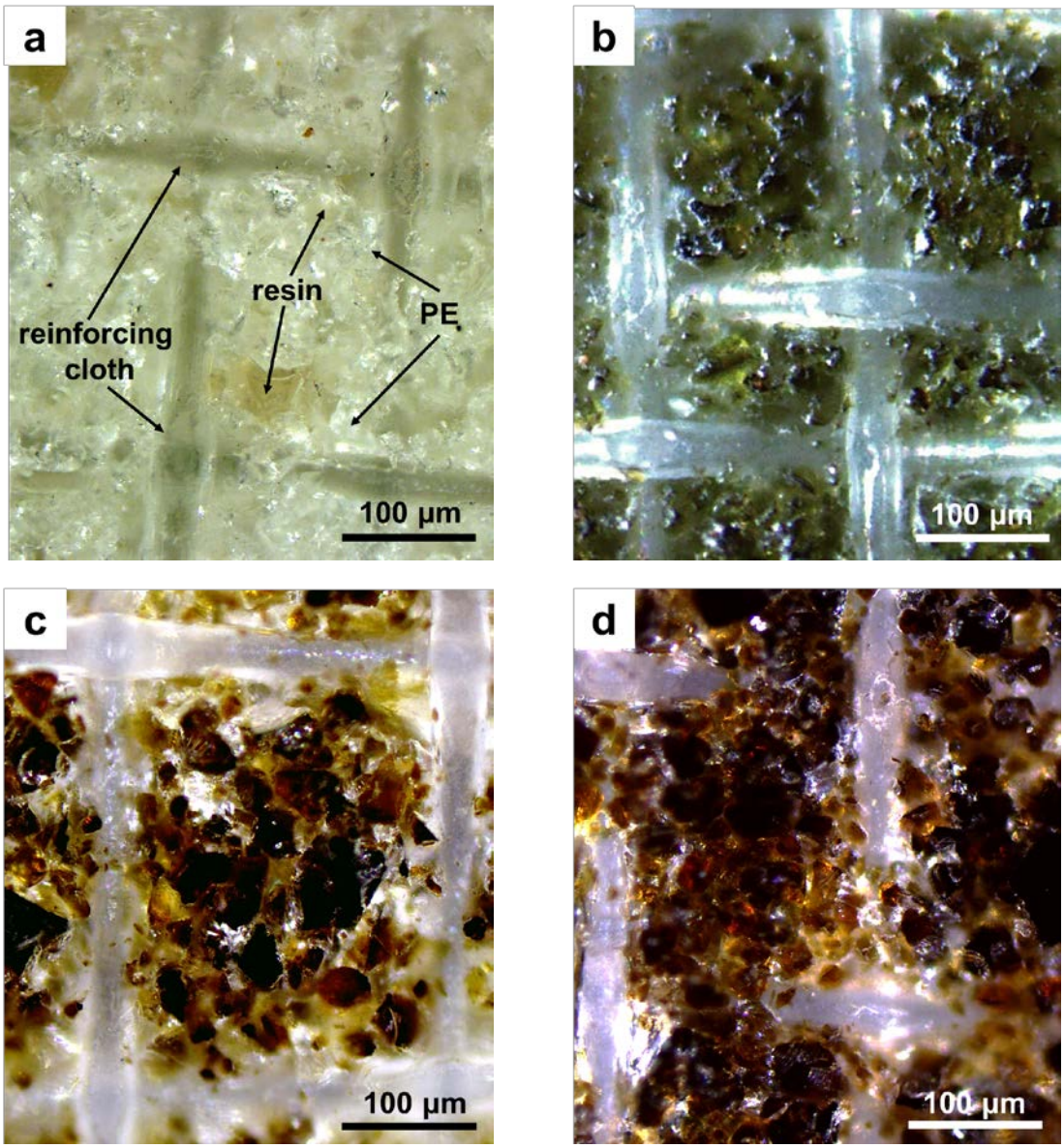

Fig. 4. Optical images of the surface of the swollen MA-41P membrane: pristine membrane in

distilled water (a); samples after 10 h of contact with an 10 mg L^{-1} anthocyanin solution (b) and wine (c); sample after 72 h of contact with wine (d). Samples (b, c, d) were stored in a buffer solution with pH= 6.68 for 1 h after the contact with anthocyanin solution or wine.

Comparison of **Figs. 3a and 3b** shows that the color of surface and bulk of the MA-41P membrane changes even after a short (3 h) contact with wine. The color depends also on the pH of the buffer solution, in which the fouled membrane was stored after the contact with wine. It is medium pink, deep amber and deep copper in the cases of pH=1.68, 6.68 and 9.18, respectively. The color of the surface is more brown, while that of the bulk is shifted to reddish (pH=1.68) or greenish-yellow (pH=6.68 and 9.18). It can be speculated that these colors are due to anthocyanins. Indeed, anthocyanins are water-soluble pigments, which depending on their pH, may change their coloration: in acidic medium (pH < 4), they exist as a red pyrile salts **[77]** and in alkaline medium (9 < pH < 11) they are in a blue quinoid or a yellow anion form **[78]**, **Fig. 3e**. Anthocyanins are rather small molecules (with a molecular mass close to 200 g $mole^{-1}$), hence, they can rapidly penetrate into an ion-exchange membrane. However, it can be seen that after 10 h of the contact with wine, the coloration of MA-41P surface shifts so that more brownish shades appear (**Fig. 4c, d**) in comparison with those in the case of pure anthocyanins (**Fig. 4b**). This change in color may reflect the appearance of tannins and anthocyanin-tannin adducts (such as catechins), which are yellow and brown, respectively **[78].** The color of MA-41P bulk (**Fig. 3**) corresponds to a color related to the anthocyanin solution with a pH shifted to the alkaline region in comparison with the solution, in which the fouled membrane was stored before taking the photos. This can be explained by the Donnan exclusion of H^+ ions as co-ions from an anion-exchange membrane **[79]**: the pH of the AEM inner solution is always more alkaline for 2 – 3 pH unities in comparison with the external solution **[49]**. Indeed, the greenish-yellow color of the bulk of MA-41P_{w10} sample stored in the solution with 6.68 (**Fig. 3b**) relates rather well to the color of the anthocyanin solution with pH=11.0 (**Fig. 3e**).

It is seen that after a short contact with wine, there is a near-surface layer in the MA-41P membrane, whose color is more intensive than the bulk; with increasing time of contact the thickness of this layer increases. After 3 h of the contact, the color of this layer is not uniform in the MA-41P. One could say, that there are regions where the depth of anthocyanin penetration into the membrane is greater and the regions with higher resistance to the anthocyanin diffusion. This difference in the depth of anthocyanin penetration can be explained by the fact that the diffusion is possible through the ion-exchange particles and the interstices between these particles and polyethylene inclusions, while polyethylene is not permeable. With increasing time

of the contact, the color of the membrane surface as well as the bulk becomes more intensive, testifying higher concentration of the pigment.

3.1.3. Results of ATR-FTIR spectroscopy

FTIR spectroscopy gives additional information about the chemical nature of foulants and their interactions with an anion-exchange membrane. A number of peaks are recorded in the IR spectra of the AMX-Sb_{w72} surface in the range from 1768 cm^{-1} to 770 cm^{-1}, which are absent in case of the pristine membrane, but are typical for wine (**Fig. 5**). In publications **[78, 80]** on the identification of wine composition, this entire range is listed as fingerprint area.

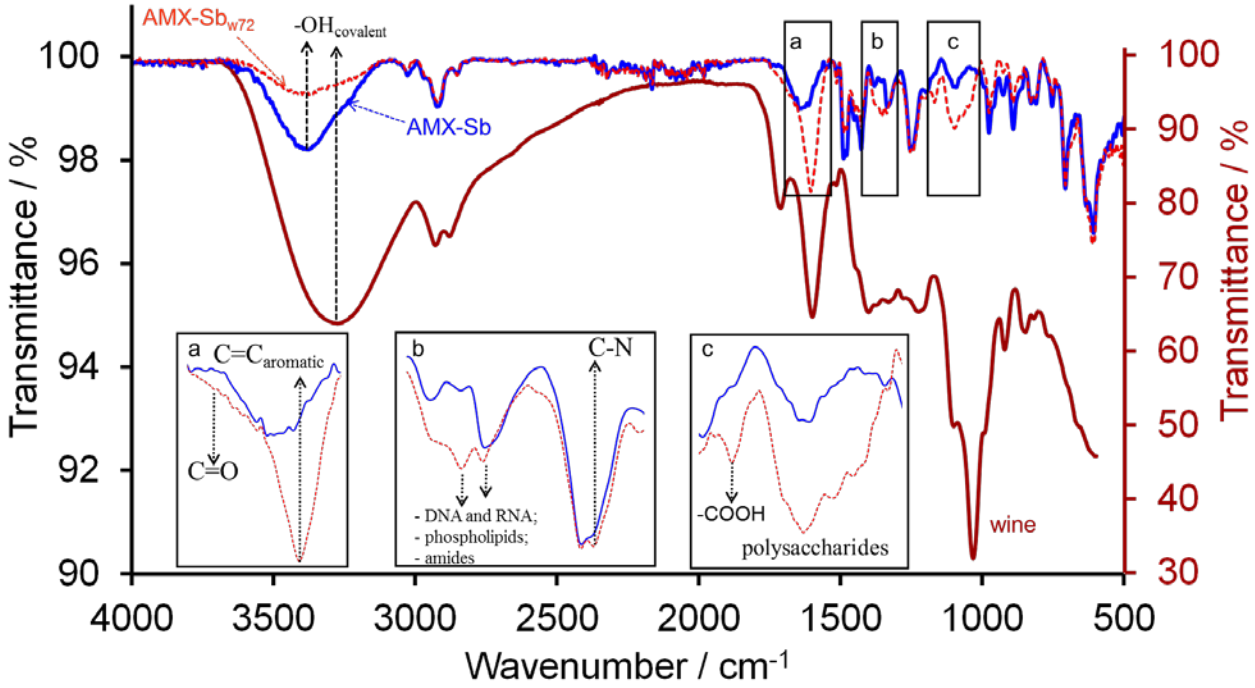

Fig. 5. FTIR spectra of the pristine membrane surface, the surface of AMX-Sb_{w72} and the wine.

The exact identification of all the wine components in the membrane is quite complicated. Therefore, we will pay attention only to some of them, which could contribute to a better understanding of fouling. In the range 1768 – 1478 cm^{-1}, there are absorption bands of amides, as well as the peaks characteristic for carbonyl groups of esters. The accumulation of organic acids inside the membrane leads to the appearance of C=O bands at about 1715 cm^{-1}, **(Fig. 5, insertion a)** and a peak at around 1167 cm^{-1}, which corresponds to –COOH groups **(Fig. 5, insertion c)**. The 1617 cm^{-1} absorption band, which is identified in the FTIR spectrum of the pristine AMX-Sb, is typical for stretching vibrations of the C = C bond of benzene rings of

divinylbenzene in the polymer matrix **[30]**. In the case of AMX-Sb_{w72}, this peak shifts to a value of 1604 cm^{-1}. Such absorption band is identified in wine spectra and is typical for stretching vibrations of the C = C bonds of benzene rings of polyphenols (anthocyanins, tannins, etc.) **(Fig. 5a)**. Besides, in the C=C spectral region (1650 – 1450 cm^{-1}), the peaks at 1450 cm^{-1}, 1475 cm^{-1}, 1480 cm^{-1} and 1510 cm^{-1} are recorded for the pristine as well for the fouled membranes. They all correspond to C=C stretching bands in aromatic rings in the polymer matrix.

The peaks in the range of 1478 – 1185 cm^{-1} indicate the presence of amides, carboxyl proteins, nucleotides (DNA and RNA) and phospholipids **(Fig. 5, insertion b)**. The peak of 1115 cm^{-1} is close to that found in wine where it is attributed to polysaccharides (glucans and mannans) [**78, 81**] **(Fig. 5, insertion c)**. However, in the case of wine (**Fig. 5**), this peak is recorded at 1105 cm^{-1}. Evidently, the shift of this peak indicates the interaction of polysaccharides with the membrane matrix.

Both for wine and for the membranes under study (both dried at 45 °C), we observe a peak in the 3300-3400 cm^{-1} range, which corresponds to the absorption band of the covalent –OH bond **(Fig. 5)**. The intensity of this peak is minimal for the initial membrane, in which trace amounts of water are apparently present, and maximal for the sample of dried wine. The latter contains not only trace amounts of water, but also a significant amount of –OH groups in polysaccharides, anthocyanins and tannins. In the case of AMX-Sb_{w72}, the intensity of this peak decreases in comparison with the wine, but increases in comparison with the initial membrane, which indicates the presence of polysaccharides, anthocyanins and tannins in the fouled membrane. The shift of the peak recorded for the AMX-Sb_{w72} sample to the region of higher wavenumber (50 cm^{-1}) compared to the wine suggests that in the membrane, the –OH groups of the foulants form hydrogen bonds with each other and with the fixed groups of ion-exchange material.

3.1.4. Contact angles and surface charge of swollen AEMs

The decrease in contact angle of the AMX-Sb and MA-41P membranes caused by their contact with wine (**Fig. 6**) evidences the adsorption of hydrated components of wine. The main changes of the contact angle in the case of AMX-Sb occur within the first 30 hours; more time is needed to stabilize the contact angle for the MA-41P membrane. The stabilization of the contact angle should mean that the formation of a relatively dense near-surface foulant layer is over, and the surface properties no longer change. As **Fig. 2c** shows, short contact with wine leads to formation of an island-like foulant layer. A longer contact causes an increase in the surface

fraction occupied by the foulant layer, hence an increase in hydrophilicity of the overall membrane surface. Since only a small part (about 20%) of the heterogeneous MA-41P membrane surface contains ion-exchange material, which adsorbs the fouling wine constituents and thus serves as initiator of the fouling process, it takes more time to form a continuous foulant layer in the case of MA-41P.

Since only a small part (about 20%) of the heterogeneous MA-41P membrane surface contains ion-exchange material, which adsorbs the fouling wine constituents and thus serves as initiator of the fouling process, it takes more time to form a continuous foulant layer in the case of MA-41P. The molecules contained in wine and forming the foulant layer (polyphenols, tannins, polysaccharides, proteins and other) are large. They include hydrophobic and hydrophilic parts. It seems that the hydrophobic parts can easier penetrate into the ion-exchange material, while the hydrophilic parts remain on the surface. Thus, the membrane surface becomes more hydrophilic. Apparently, the AV-17-2P anion-exchange macroporous resin contained in the MA-41P membrane allows greater sorption of the hydrophobic parts of the foulant molecules than the AMX-Sb membrane, which explains higher hydrophilization of the MA-41P surface during its contact with wine.

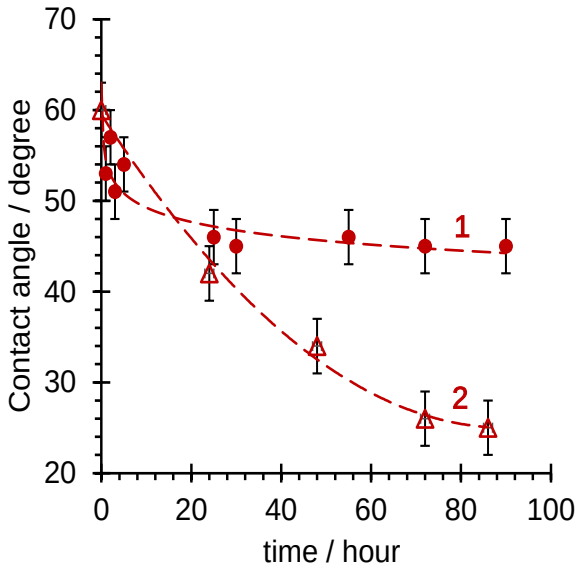

Fig. 6. Dependence of the contact angle of AMX-Sb (1) and MA-41P (2) membranes upon the duration of its soaking in wine.

The surface charge of the sample, which contacted with wine for 72 hours, is essentially smaller in absolute value than that of the pristine membrane (**Fig. 7**). The sign of charge of the AMX-Sb_{w72} membrane surface depends on the pH of the solution, where the membrane was

stored in after its contact with wine: if the fouled membrane was kept in acidic media (pH = 3.5) prior to electrokinetic measurements, then the sign of its charge remains the same as it was for the pristine membrane (positive); and when the membrane was kept in neutral solution (pH = 6.7), its surface charge changes to negative.

The surface charge of the fouled membrane is apparently determined by the foulant layer well seen in **Figs. 2c-2f**. It seems that this layer screens the own fixed groups of the membrane, which are positively charged. The charge of the foulant layer surface is pH-dependent: it should involve the groups, which are negatively charged at a neutral pH, while can be protonated and become positively charged at a low pH.

Note that the charge determined by electrokinetic measurements refers to true surface area **[66]**.

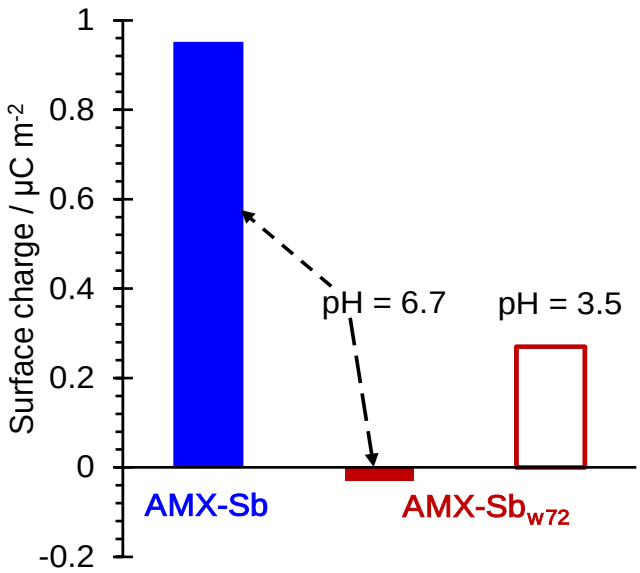

Fig. 7. Surface charge of the pristine AMX-Sb membrane equilibrated with a 0.02 M NaCl solution (pH=6.7) and the sample, which contacted with wine for 72 hours and then was stored for 24 hours in NaCl solutions with pH=6.7 or pH=3.5

Analysis of the data presented above allowed us to suggest the following hypothesis about the sequence of events occurring when an anion-exchange membrane is fouled with wine. During the first hours of contact, strongly hydrated and relatively small organic molecules penetrate into the membrane pores, causing their stretching, an increase in membrane thickness and a sharp decrease of contact angle. These molecules may include anions of organic acids. Judging by the observed changes in coloration and their dependence on pH, anthocyanins (which are rather mobile with their molecular mass close to 200 g mole^{-1}**)** might be a significant part of

these molecules. When the pores are expanded, tannins, proteins and other high molecular substances with low diffusivity can enter the membrane, causing a further increase in its thickness. The presence of chromene cycles, which are characteristic of anthocyanins and condensed tannins (catechins), at membrane / solution interface, may cause the observed changes in surface charge. In acidic medium, the chromene cycles exist in form of positively charged flavylium cations **[77]**, which could contribute to the positive charge of the foulant layer. In neutral medium, these cycles transform into chalcone or quinonoid pseudo-bases, which do not possess electric charge **[77]**. A small negative charge of AMX-Sb_{w72} surface is presumed to be caused by partially dissociated hydroxyl and carboxyl groups, which are present in the formed surficial colloidal aggregates. The subsequent formation of branched strongly hydrated colloidal structures in large pores and on the AEM surface is apparently similar to those observed in the case of micro- and ultrafiltration membranes fouled with wine **[27,33,34,35,36,38,39,40,45]**.

As it was shown by Bazinet et al. **[49,50]**, the main interactions governing the fouling of anion-exchange membrane by organic acids presented in wine and juices, are of the electrostatic nature. Some of the hydroxyl groups of tannins and the carboxyl groups of organic acids in wine are deprotonated due to elevated pH of the internal solution, which causes a negative charge of these acids **[82]**. Additionally, there are chemical interactions, which have an essential impact on the AEM behavior in wine and juices. The aromatic matrix of studied membranes affects the introduction of polyphenols into the AEM volume as well as their adsorption on the AEM surface due to π-π (stacking) interactions between the benzene rings (present in membrane matrix) and phenol rings (components of anthocyanins and tannins) **[27]**. Besides, the hydrogen bonds can be formed between tertiary or secondary amino groups of an AEM **[76]** and hydroxyl (carboxyl) groups of anthocyanins, tannins and other components of wine **[83]**.

3.2. Current-voltage curves and pH changes

CVCs of studied samples as well as differences in pH between the desalination channel inlet and outlet are shown in **Fig. 8.** The desalination channel is formed by one of the AEMs under study and a MK-40 cation-exchange membrane. CVCs show the potential drop through the membrane under study (the Luggin measuring capillaries are introduced close to the left and right membranes sides) versus the current density normalized to the theoretical limiting current density, i_{lim}^{theor}, calculated using the Lévêque equation, Eq. (1). The reduced potential drop defined by Eq. (2) is used. The characteristics of CVCs are given in **Table 4**. Their determination is explained in **Fig. 8b.** The experimental current density, i_{lim}^{exp}, is determined by the point of

intersection of the tangent drawn to the CVC plateau and the ordinate. The plateau length is determined as in Ref. **[84]**, **Fig. 8b**. The plateau slope is found as the $\Delta i_p/\Delta\varphi_p$ ratio, the meaning of Δi_p and $\Delta\varphi_p$ is clear from **Fig. 8b**.

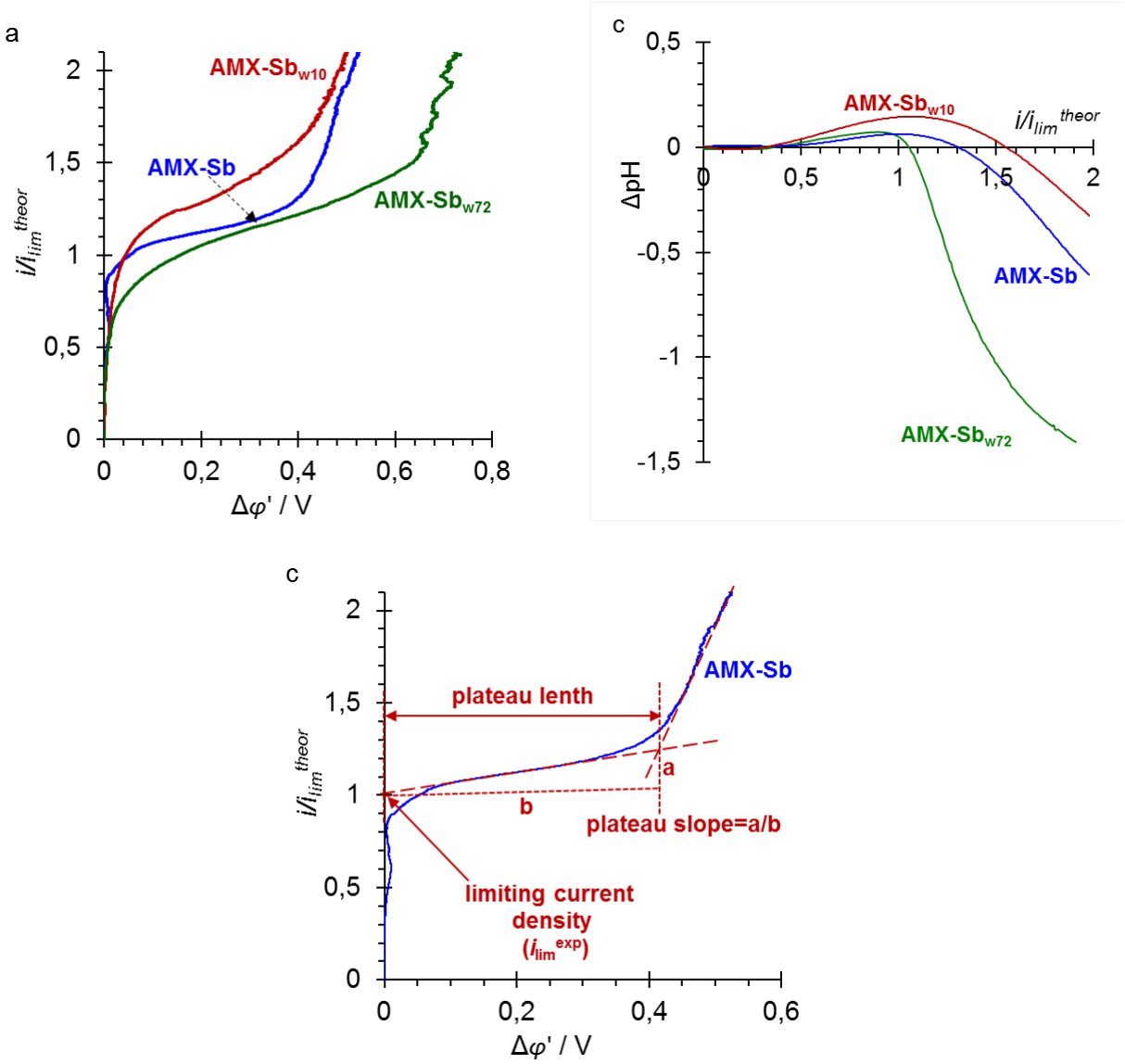

Fig. 8. *I-V* curves for a pristine AMX-Sb membrane and the samples contacted with wine for 10 h (AMX-Sb$_{w10}$) and 72 h (AMX-Sb$_{w72}$) (a), as well as the pH difference between the desalination compartment outlet and inlet vs i / i_{lim}^{theor} (c); (b) defines the characteristic values of the *I-V* curve. A 0.02 M NaCl was used as the feed solution.

Table 4. Characteristics of *I-V* curves, diffusion layer thickness and water splitting rate. The latter is expressed by the OH^- ion transport number in the AEM. The effective diffusion layer thickness, δ_N, found using Eq. (3), is given for different values of the reduced potential drop, $\Delta\varphi'$, (Eq. (2), to compare with δ_{Lev}=239 μm, calculated using Eq. (1).

Membrane	i_{lim}^{exp} / i_{lim}^{theor}	i_{lim}^{exp}, mA cm^{-2}	Plateau length, mV	Plateau slope, mS cm^{-2}	*at* $\Delta\varphi'$=0.1 V		at $\Delta\varphi'$=0.5 V	
					δ_N, μm,	T_{OH}	δ_N, μm	T_{OH}
AMX-Sb	1.0	2.9	410	0.56	216	0.13	152	0.16
AMX-Sb$_{w10}$	1.1	3.2	400	1.13	217	0.10	144	0.09
AMX-Sb$_{w72}$	0.9	2.6	640	0.80	-	-	-	-

As it can be seen from **Fig. 8a** and **Table 4**, a short contact (10 h) of the AMX-Sb membrane with wine leads to an increase in the values of i_{lim}^{exp}. As well, the plateau length decreases and the plateau slope increases, which signifies that the overlimiting conductance increases. At the same time, the pH of the outlet solution is higher than that in the case of the non-fouled AMX-Sb membrane. The variation of pH between the inlet and outlet solutions is caused by the difference in the rate of water splitting at the AEM and CEM. Water splitting at the depleted interface of the AEM generates H^+ and OH^- ions; the OH^- ions pass through the AEM into the concentrate compartment, while the H^+ ions go towards the bulk of desalination channel. The depleted interface of the CEM generates the H^+ ions, which pass through the CEM into the concentrate compartment, and OH^- ions, which go towards the bulk of desalination channel. **Fig. 8c** shows that at low current densities, the outlet solution pH is higher than the inlet solution pH. This signifies that water splitting rate at the CEM is higher than that at the AEM. The cause is that the limiting current density at the CEM in NaCl solutions is about 1.5 times lower than that at the AEM, which is due to the lower diffusivity of Na^+ compared to Cl^-. Hence, the limiting current density at the CEM is reached, when i / i_{lim}^{theor} for the AEM is about 0.6. As a heterogeneous MK-40 membrane is used as the CEM in our ED cell, the local limiting current density at the conductive surface regions is attained even at lower values of i / i_{lim}^{theor} (funnel effect **[85]**). However, when the value of i / i_{lim}^{theor} is sufficiently high, the desalted solution is acidified (**Fig. 8c**), which is due to higher water splitting at the AEM. The latter is explained by the fact that at a relatively high concentration polarization the water splitting rate is governed by the catalytic participation of membrane functional groups, which accelerate protonation-deprotonation reactions of water **[86;87]**. The MK-40 membrane contains sulfo-groups characterized by a very low catalytic activity towards water splitting reaction **[86,87]**. The AMX-Sb membrane contains mainly quaternary ammonium, but a certain amount of tertiary and secondary amino groups **[88]**, the latter showing a strong catalytic activity towards water splitting **[86,87]**.

Thus, examining **Fig. 8c** allows one to conclude that the water splitting rate at the AMX-Sb$_{w10}$ is lower than that at the AMX-Sb membrane, since the CEM membrane forming the desalination channel together with the AEM under study is the same (MK-40) in both cases. This

conclusion is confirmed by the measurement of the effective transport numbers of OH^- ions, T_{OH}, in the AEMs. (The method of T_{OH} determination is described in Section 2.2.) The value of T_{OH}, found at $i / i_{lim}^{theor} = 1.5$ ($\Delta\varphi'$=0.5 V) is equal to 0.16 ± 0.05 for the AMX-Sb and 0.09 ± 0.05 for the AMX-Sb_{w10} (**Table 4**).

The observed changes in the CVC, in the absence of intensive water splitting, may occur only due to enhanced mass transfer caused by current induced convection. As the electrolyte concentration in the feed solution is low (0.02 M NaCl), the expected contribution of gravitational convection is low [**89,90**]. However, electroconvection in similar conditions could enhance mass transfer significantly [**91,66**]. The effect of electroconvection on the mass transfer rate is often evaluated by the value of effective thickness of diffusion boundary layer, δ_N, entering the following equation [**92**]:

$$\left|i_{Cl}\right| = \frac{2FD_{Cl}C_{Cl}}{\delta_N} + \frac{D_{Cl}}{D_H}\left|i_H\right| \qquad (3)$$

where i_{Cl} and i_H are the partial current densities of Cl^- and H^+ in the depleted diffusion layer, respectively, D_{Cl^-} = 2.04 10^{-5} cm^2 s^{-1} and D_H = 9.34 10^{-5} cm^2 s^{-1} are the diffusion coefficients of Cl^- and H^+ in solution, respectively. The absolute values are used in Eq. (3) in order to avoid the confusion with the sign of i_{Cl} and i_H. Eq. (3) is deduced with taking into account the exaltation current due to the flux of H^+ ions generated at the AEM depleted surface, which "exalts" the Cl^- transport from the feed solution bulk. The increase ("exaltation") in the Cl^- current density is caused by the electrostatic forces of attraction between the H^+ ions produced in water splitting and located near the depleted surface and the Cl^- ions in the bulk feed solution **[92,93]**. The diffusion layer of effective thickness δ_N, acts a similar role as the Nernst diffusion layer, which controls the mass transfer rate at underlimiting current density **[94]**.

The value of δ_N may be found from Eq. (3), when the partial current densities, i_{Cl} and i_H, are known from the experiment. i_{Cl} is expressed as $T_{Cl}i_{over\,lim}$, i_H as $T_{OH}i_{over\,lim}$, where $i_{over\,lim}$ is a given overlimiting current density, while T_{Cl} and T_{OH} are the effective transport number of Cl^- and OH^- ions in the membrane found for this current density; $T_{Cl} + T_{OH} = 1$ (**Table 4**). It is taken into account that the partial current density of H^+ ions in the depleted diffusion layer is equal to the partial current density of OH^- ions in the AEM. The estimation of δ_N shows that its value at low concentration polarization (CP) ($\Delta\varphi'$=0.1 V) is close to that found using the Lévêque equation (1). However, δ_N for AMX-Sb_{w10} is lower than that for AMX-Sb. At higher

CP (i=1.5 i_{lim}^{theor}) the difference between these values increases. It can be suggested basing on the results of Refs. **[66,91]** that at low CP electroconvection occurs as electroosmosis of the first kind **[95,96]**, while at higher CP, it is nonequilibrium unstable electroconvection of Rubinstein-Zaltzman mode **[97]** with a great contribution of electroosmosis of the second kind **[98,99]**. The onset of electroconvection instability occurs at $\Delta\varphi'$ close to 0.4 V, where the slope of *I-V* curve becomes steeper and oscillations of potential drop appear (**Fig. 7a**). (Note that in the experiment, the current density is swept with a constant rate of 35.7 mA h^{-1}). One can see that the beginning of the steeper slope occurs at a higher current density in the case of AMX-Sb_{w10}, hence, the current (and mass transfer) increase owing to electroosmosis of the first kind is essentially higher in the case of AMX-Sb_{w10} when compared to the AMX-Sb. Apparently it is due to the surface heterogeneity induced by the deposition of wine components' aggregates. Perhaps, an increase in surface waviness discussed in Section 3.1.1 (**Table 2**) may also contribute to in enhancement of electroconvection. This electric and geometric heterogeneity leads to the appearance of tangential electric force enhancing electroosmosis **[100,101,96]**. It is interesting that the water contact angle decreases with increasing degree of surface fouling; that signifies that the low conducting spots of wine components' aggregates are of hydrophilic nature. When comparing with the case where the low conducting spots on the AMX membrane surface are hydrophobic **[66,91]**, one can state that there is no essential difference in the behavior of the modified membranes at $\Delta\varphi' > 0.4$ V, where electroosmosis of the first kind is well developed and passes to electroosmosis of the second kind. However, in the initial stages of electroconvection when electroosmosis of the first kind only becomes noticeable ($\Delta\varphi' \approx 20 - 50$ mV), the difference is essential. One can see that on the *I-V* curve of the AMX-Sb membrane in the above mentioned interval of $\Delta\varphi'$ there is a small protrusion directed to the vertical axis and characterized by the fact that with increasing current density, the value of $\Delta\varphi'$ decreases instead of normally expected increase. We link this decrease in $\Delta\varphi'$ with onset of electroconvection bringing fresh solution from the bulk to the depleted interface and evacuating from this interface depleted solution **[66**Ошибка! Закладка не определена.**,91]**. **Fig. 8a** shows that this protrusion disappears when hydrophilic wine components' aggregates form on the AMX-Sb surface. However, the deposition of hydrophobic spots on the AMX surface results in an increase of this protrusion. It can be so important that a current density equal to 1.2 i_{lim}^{theor} passes at $\Delta\varphi' \approx$20 mV, and a current density equal to 1.4 i_{lim}^{theor} passes at $\Delta\varphi' \approx$20 mV **[91]**. A local maximum on the chronopotentiogram of such a modified membrane arises at $\Delta\varphi' \approx$20 - 30 mV followed by a local minimum, which can drop to $\Delta\varphi' \approx$ 1 mV [**91**], making one to assume that these early

oscillations are due to equilibrium electroconvective instability recently predicted theoretically by Rubinstein and Zaltzman **[96]**.

A longer contact of the AMX-Sb membrane with wine causes a significant decrease in the i_{lim}^{exp} value (the characteristics of AMX-Sb_{w72} in **Fig. 8a** and **Table 4**). It is accompanied by an increase in the plateau length and a decrease in its slope on the CVC as well as by a decrease in the overlimiting current density compared to those obtained for the AMX-Sb and AMX-Sb_{w10} membranes (**Fig.8a**, **Table 4**). The reason for the decrease in i_{lim}^{exp} is most likely the reduction of electroconvection. This reduction may be caused by a significant decrease in the surface charge (**Fig. 7**), which leads to a decrease in electroosmosis of the first kind **[95,97,102]** important at $i \leq i_{lim}^{exp}$ **[91,66**Ошибка! Закладка не определена.**]**. Another cause may be due to transformation of the surface structure from an island-like one (after 10 h of fouling) to a homogeneous one: nearly all the surface of the AMX-Sb_{w72} membrane is covered with the deposit of wine components' aggregates (**Fig. 2e**). In addition, intensive water splitting at the AMX-Sb_{w72} surface can also reduce electroconvection: the appearance of H^+ ions in the depleted solution near the interface decreases the space charge density (negative in the case of AEM) **[103]**.

A strong acidification of the desalination channel outlet solution in the case of AMX-Sb_{w72} membrane evidences that an intensive water splitting at the AMX-Sb_{w72} surface starts immediately after the limiting current density is reached (**Fig. 8b**). The cause for increasing water splitting rate may be formation of a bipolar membrane structure due to the foulant layer. **Fig. 7** shows that in the case where the AMX-Sb_{w72} membrane is bathed in a 0.02 M NaCl solution (which is used in voltammetric measurements), the charge of its surface is negative, while it is positive for the pristine membrane. Note that the membrane bulk remains pristine after 72 h of the contact with wine. The negative surface charge may be due to native structures of microorganisms found on the surface (**Fig. 1c**), which contain negatively charged carboxylic and phosphoric acid groups in nucleotides (DNA and RNA) and phospholipids. Carboxyl groups are contained also in foulant constituents such as organic acids and proteins. The FTIR analysis (**section 3.1.3**.) shows that carboxylic and phosphoric groups are absent in the pristine membrane, while they appear in the near-surface layer of AMX-Sb_{w72} membrane. In addition to their negative charge, the carboxylic and phosphoric groups are known as effective catalyzers of water splitting reaction **[86,104]**. Similar effects of increasing water splitting caused by the contact of IEMs with protein-containing solution are described in literature by Park et al. **[105]**, who studied the impact of BSA, and by Slouka et al. **[106]**, who shown that DNA molecules on the surface of an AEM contributed to increasing water splitting and electroconvective vortex

suppression. The formation of a bipolar membrane structure is also possible under electric current due to precipitation of hydroxides of multivalent cations on the depleted membrane surface **[107]**.

Thus, voltammetry and pH measurements show intensification of electroconvection and weakening of water splitting in the case of a short-term contact of the AMX-Sb membrane with wine. However, a long-term contact of this membrane with wine leads to suppression of electroconvection and an increase in water splitting.

4. Conclusion

The contact of AEMs with wine results in deterioration of membrane properties. A long-term contact leads to a decrease in ion-exchange capacity and conductivity, while the water content and membrane thickness increase **[30,55]**. However, a short-term contact has an unexpected effect. While a 10-hour contact with wine causes a two-fold increase in the AMX-Sb membrane ohmic resistance, some electrochemical properties of the fouled membrane are improved: water splitting at the membrane surface is partially suppressed, electroconvection is enhanced, as well as the mass transfer rate in overlimiting current regime. This improvement is governed by changes of the surface properties and is apparently due to the foulant openwork layer formed by aggregates of wine constituents on the membrane surface. The aggregates are highly hydrated colloidal structures, which involve, according to the FTIR analysis, anthocyanins, tannins, amino acids, polysaccharides and proteins. Their surface contains the groups, which are negatively charged at a neutral pH, while can be protonated and become positively charged at a low pH.

The island-like structure of the foulant layer leads to the appearance of tangential electric force producing electroosmotic lateral flow due to appearance of electric heterogeneity. Increasing surface roughness/waviness can also contribute to enhancing electroosmosis. Electroconvection develops despite the noticeable hydrophilization of the AMX-Sb surface by the highly hydrated aggregates of wine constituents. The intensity of electroconvection at relatively high voltage is comparable with the case where the low-conducting hydrophobic spots are introduced on the AMX-Sb membrane surface **[91]**. However, at low voltage ($\Delta\varphi'$<40 mV), electroconvection in the case of hydrophobic spots is essentially more intensive than electroconvection developed due to the hydrophilic aggregates of the foulant. Hence, our results confirm the results of other authors **[108,109]** that the membrane surface heterogeneity, within certain limits, together with surface waviness **[66,97]**, enhances electroconvection. An important

new finding consists in the fact that the degree of hydrophobicity affects electroconvection mainly at low voltages. With increasing voltage, electroconvection tends to be unstable, then the degree of hydrophobicity acts a secondary role.

The color of membrane bulk in initial stages of membrane fouling by wine is determined by the anthocyanin species, which have relatively low molecular mass. At later stages, larger molecules of tannins, proteins and other wine constituents penetrate into the membrane leading to essential loss of conductivity. The Donnan exclusion of the H^+ ions as co-ions from the membrane shifts pH of the internal solution to alkaline region, which causes deprotonation of anthocyanins and tannins and their transformation into negatively charged forms. These changes in the anthocyanin and tannin form can be observed due to changes in the membrane bulk color. The shift in the charge of sorbed species leads to a partial loss of membrane exchange capacity caused by the electrostatic interactions of negatively charged groups of sorbed species and positively charged fixed groups of the AEM. The subsequent contact of the membrane with wine leads to increasing and thickening of the foulant layer. It becomes rather uniformly distributed over the surface and 2 – 3 μm thick after 72 hours of contact of the AMX-Sb with wine. The presence of this layer, as well as biofouling of the AMX-Sb_{w72} simple lead to an increase in water splitting and a reduction of electroconvection.

The wine is a very complicated system containing a large number of components. However, the components, which mainly affect the behavior of ion-exchange membranes, can be now specified; they are polyphenols and polysaccharides as suggested in literature [**26-29, 54**] and confirmed in our study. Nevertheless, many important details of the impact of different components remain unclear. It seems that the best strategy, as it was suggested by an anonymous Reviewer of our paper, is to study the membrane behavior separately using each of the main components. With that, it should be taken into account that due to different chemical affinity between different components and the membrane matrix, the membrane behavior in a mixture of wine components could have some features in comparison to the cases where only individual components are present. This affinity may be due to π-π (stacking) interactions **[27]** between phenol rings of polyphenols and aromatic groups of membrane matrix, van der Waals attraction forces **[35, 41]** and other kinds of interactions. This way could lead to clearer answers about the mechanisms of membrane fouling in wine and other complicated organic products, kinetics of species transport and other questions.

Acknowledgements

The research was supported by Russian Science Foundation (project № 17-19-10305). The authors thank also the Center for Collective Use of the Kuban State University "Diagnostics of the structure and properties of nanomaterials" and “Eco-analytical Center of Kuban State University” for the scientific equipment provided.

References

[1] Y. El Rayess, M. Mietton-Peuchot, Membrane technologies in wine industry: an overview, Crit. Rev. Food Sci. Nutr. 56 (2016) 2005.

[2] A.Y. Tamime, Membrane processing: dairy and beverage applications, John Wiley & Sons, UK, 2012.

[3] S.V. Corti, S.C. Paladino, Tartaric stabilization of wines: comparison between electrodialysis and contact cold treatment [Estabilización tartárica en vinos: Comparación entre electrodiálisis y tratamiento de frío por contacto], Revista de la Facultad de Ciencias Agrarias 48 (2016) 225 – 238.

[4] M.N. De Pinho, Membrane processes in must and wine industries, Membr. Technol.: Membr. Food Appl. 3 (2010) 105–118.

[5] G. Daufin, J.-P. Escudier, H. Carrere, S. Berot, L. Fillaudeau, M. Decloux, Recent and emerging applications of membrane processes in the food and dairy industry, Food Bioprod. Process. 72 (2001) 89–102.

[6] B. Gautier, Une nouvelle approche révolutionnaire et performante de la filtration tangentielle des vins, Revue des oenologues et des techniques vitivinicoles et oenologicques: Magazine trimestriel d'information professionnelle 30 (2003) 27–30.

[7] A. Vernhet, A. Grangeon, Innovations dans la microfiltration des vins: membranes et procédés, Revue des oenologues et des techniques vitivinicoles et oenologicques: Magazine trimestriel d'information professionnelle 31 (2004) 37–40.

[8] G. Thoukis, Chemistry of wine stabilization: a review, Advances in chemistry series, A. Dinsmoor Webb (Ed.), Chemistry of Wine Making, American Chemical Society, Washington, 1974.

[9] P. Ribéreau - Gayon, Y. Glories, A. Maujean, D. Dubourdieu, Handbook of enology: the chemistry of wine, Stabilization and Treatments, 2nd ed., Volume 2: Dunod, Paris, 2006.

[10] A.M. Romanov, V.I. Zelentsov, Use of electrodialysis for the production of grape-based soft and alcoholic drinks, Surf. Eng. Appl. Elect. 43 (2007) 279–286.

[11] C. Riponi, F. Nauleau, A. Amati, G. Arfelli, M. Castellari, Essais de stabilisation tartrique des vins au moyen de l'électrodialyse, Rev. Franç. d'Œnol. 137 (1992) 59–63.

[12] L.-L. Low, B. O'Neill, C. Ford, J. Godden, M. Gishen, C. Colby, Economic evaluation of alternative technologies for tartrate stabilisation of wines, Int. J. Food Sci. Tech. 43 (2008) 1202–1216.

[13] R. Audinos, J.P. Roson, C. Jouret, Application of electrodialysis to the elimination of certain grape juice and wine components, Connaissance de la Vigne et du Vin 13 (1979) 229–239.

[14] L. Paronetto, L. Paronetto, A. Braido, Some tests on tartrate stabilization of musts and wines by electrodialysis, Vignevini 4 (1977) 9–15.

[15] C. Lasanta, J. Gomez, Tartrate stabilization of wines, Trends Food Sci. Tech. 28 (2012) 52–59.

[16] M. Moutounet, J.-L. Escudier, B. Saint-Pierre, In les acquisitions r´ecentes dans les traitements physiques du vin (ed. B. Don`eche), Paris: Tec. et Doc., Lavoisier, 1994.

[17] F. Gonçalves, C. Fernandes, P. Cameira dos Santos, M.N. De Pinho, Wine tartaric stabilization by electrodialysis and its assessment by the saturation temperature, J. Food Eng., 59 (2003) 229–235.

[18] J. Gómez Benítez, V.M. Palacios Macías, P. Szekely Gorostiaga, R. Veas López, L. Pérez Rodríguez, Comparison of electrodialysis and cold treatment on an industrial scale for tartrate stabilization of sherry wines, J. Food Eng. 58 (2003) 373–378.

[19] E. Serre, E. Rozoy, K. Pedneault, S. Lacour, L. Bazinet, Deacidification of cranberry juice by electrodialysis: impact of membrane types and configurations on acid migration and juice physicochemical characteristics, Sep. Purif. Technol. 163 (2016) 228–237.

[20] A. Cassano, N.K. Rastogi, A. Basile, Membrane technologies for water treatment and reuse in the food and beverage industries, Adv. Membr. Tech. Water Treat. (2015) 551–580.

[21] I.S. Arvanitoyannis, D. Ladas, A. Mavromatis, Wine waste treatment methodology, Int. J. Food Sci. Tech. 41 (2006) 1117–1151.

[22] L. Bazinet, A. Doyen, Antioxidants, mechanisms, and recovery by membrane processes, Crit. Rev. Food Sci. Nutr. 57 (2017) 677–700.

[23] A. Giacobbo, A.M. Bernardes, M.N. de Pinho, Sequential pressure-driven membrane operations to recover and fractionate polyphenols and polysaccharides from second racking wine lees, Sep. Purif. Technol. 173 (2017) 49–54.

[24] S. Mikhaylin, L. Bazinet, Fouling on ion-exchange membranes: Classification, characterization and strategies of prevention and control, Adv. Colloid Interface Sci. 229 (2016) 34–56.

[25] R. S. Jackson, Wine science: principles and applications, 4 ed. London: Academic Press, 2014.

[26] C. Poncet-Legrand, D. Cartalade, J.-L. Putaux, V. Cheynier, A. Vernhet, Flavan-3-ol Aggregation in Model Ethanolic Solutions: Incidence of Polyphenol Structure, Concentration, Ethanol Content, and Ionic Strength, Langmuir 19 (2003) 10563–10572.

[27] M. Ulbricht, W. Ansorge, I. Danielzik, M. König, O. Schuster, Fouling in microfiltration of wine: The influence of the membrane polymer on adsorption of polyphenols and polysaccharides, Sep. Purif. Technol. 68 (2009) 335–342.

[28] S.S. Madaeni, T. Mohamamdi, M.K. Moghadam, Chemical cleaning of reverse osmosis membranes, Desalination 134 (2001) 77–82.

[29] N. Cifuentes-Araya, G. Pourcelly, L. Bazinet, How pulse modes affect proton-barriers and anion-exchange membrane mineral fouling during consecutive electrodialysis treatments, J. Colloid Interf. Sci. 392 (2013) 396–406.

[30] R. Ghalloussi, W. Garcia-Vasquez, L. Chaaban, L. Dammak, C. Larchet, S.V. Deabate, E. Nevakshenova, V. Nikonenko, D. Grande, Ageing of ion-exchange membranes in electrodialysis: A structural and physicochemical investigation, J. Membr. Sci. 436 (2013) 68 – 78.

[31] A. Cassano, E. Drioli, Integrated Membrane Operations: In the Food Production, De

Gruyter, Berlin, 2013.
[32] P. Aimar, P. Bacchin, Slow colloidal aggregation and membrane fouling, J. Membr. Sci. 360 (2010) 70–76.
[33] A. Vernhet, P. Pellerin, M.-P. Belleville, J. Planque, M. Moutounet, Relative impact of major wine polysaccharides on the performances of an organic microfiltration membrane, Am. J. Enol. Vitic. 50 (1999) 51–56.
[34] P. Blanpain, M. Lalande, Investigation of fouling mechanisms governing permeate flux in the crossflow microfiltration of beer, Filtr. Sep. 34 (1997) 1065–1069.
[35] H. Susanto, Y. Feng, M. Ulbricht, Fouling behavior of aqueous solutions of polyphenolic compounds during ultrafiltration, J. Food Eng. 91 (2009) 333–340.
[36] H.M. Lappin-Scott, J.W. Costerton, Bacterial biofilms and surface fouling, Biofouling 1 (1989) 323–342.
[37] A.W. Zularisam, A. Ahmad, M. Sakinah, A.F. Ismail, T. Matsuura, Role of natural organic matter (NOM), colloidal particles, and solution chemistry on ultrafiltration performance, Sep. Purif. Technol. 78 (2011) 189–200.
[38] J.A. Koehler, M. Ulbricht, G. Belfort, Intermolecular forces between a protein and a hydrophilic modified polysulfone film with relevance to filtration, Langmuir 16 (2000) 10419–10427.
[39] P. Czekaj, F. López, C. Güell, Membrane fouling during microfiltration of fermented beverages, J. Membr. Sci. 166 (2000) 199–212.
[40] A. Vernhet, D. Cartalade, M. Moutounet, Contribution to the understanding of fouling build-up during microfiltration of wines, J. Membr. Sci. 211 (2003) 357–370.
[41] T. Tadros, Encyclopedia of colloid and interface science, Springer, 2013.
[42] N-H Lee, G. Amy, J-P Croué, H. Buisson, Identification and understanding of fouling in low-pressure membrane (MF/UF) filtration by natural organic matter (NOM), Water Res. 38 (2004) 4511-4523.
[43] F. Wang, V.V. Tarabara, Pore blocking mechanisms during early stages of membrane fouling by colloids, Adv. Colloid Interface Sci. 328 (2008) 464-469.
[44] R.G.M. van der Sman, H.M. Vollebregt, A. Mepschen, T.R. Noordman, Review of hypotheses for fouling during beer clarification using membranes, J. Membr. Sci. 396 (2012) 22–31.
[45] J.S. Baker, L.Y. Dudley, Biofouling in membrane systems – a review, Desalination 118 (1998) 81–89.

[46] J. Wingender, H.C. Flemming, Biofilms in drinking water and their role as reservoir for pathogens, Int. J. Hyg. Environ. Health 214 (2011) 417–423.
[47] C. Flanzy, OEnologie: fondements scientifiques et technologiques, Paris: Lavoisier TEC&DOC, 1998.
[48] S. Suwal, A. Doyen, L. Bazinet, Characterization of protein, peptide and amino acid fouling on ion-exchange and filtration membranes: review of current and recently developed methods, J. Membr. Sci. 496 (2015) 267–283.
[49] M.-E. Langevin, L. Bazinet, Ion-exchange membrane fouling by peptides: A phenomenon governed by electrostatic interactions, J. Membr. Sci. 369 (2011) 359–366.
[50] M. Persico, S. Mikhaylin, A. Doyen, L. Firdaous, V. Nikonenko, N. Pismenskaya, L. Bazinet, Prevention of peptide fouling on ion-exchange membranes during electrodialysis in overlimiting conditions, J. Membr. Sci. 543 (2017) 212–221.
[51] A. Bukhovets, T. Eliseeva, Y. Oren, Fouling of anion-exchange membranes in electrodialysis of aromatic amino acid solution, J. Membr. Sci. 364 (2010) 339–343.
[52] M. Higa, N. Tanaka, M. Nagase, K. Yutani, T. Kameyama, K. Takamura, Y. Kakihana, Electrodialytic properties of aromatic and aliphatic type hydrocarbon-based anion-exchange membranes with various anion-exchange groups, Polymer 55 (2014) 3951–3960.
[53] N. Tanaka, M. Nagase, M. Higa, Organic fouling behavior of commercially available hydrocarbon-based anion-exchange membranes by various organic-fouling substances, Desalination 296 (2012) 81–86.
[54] R. Audinos, Fouling of ion-selective membranes during electrodialysis of grape must, J. Membr. Sci. 41 (1989) 115–126.
[55] W. Garcia-Vasquez, L. Dammak, C. Larchet, V. Nikonenko, N. Pismenskaya, D. Grande, Evolution of anion-exchange membrane properties in a full scale electrodialysis stack, J. Membr. Sci. 446 (2013) 255–265.
[56] R. Ghalloussi, L. Chaabane, L. Dammak, D. Grande, Ageing of ion-exchange membranes used in an electrodialysis for food industry: SEM, EDX and limiting current investigations, Desalin. Water Treat. 56 (2015) 2561–2566.
[57] W. Garcia-Vasquez, L. Dammak, C. Larchet, V. Nikonenko, D. Grande, Effects of acid-base cleaning procedure on structure and properties of anion-exchange membranes used in electrodialysis, J. Membr. Sci. 507 (2016) 12–23.
[58] Astom corporation ion exchange membranes, (n.d.).
http://www.astomcorp.jp/en/product/10.html.

[59] United Chemical Company Shchekinoazot. Products.
http://www.azotom.ru/monopolyarnye-membrany/
[60] X.T. Le, Permselectivity and microstructure of anion exchange membranes, J. Colloid Interface Sci. 325 (2008) 215 – 222
[61] V.I. Vasil'eva, E.M. Akberova, V.I. Zabolotskii, Electroconvection in systems with heterogeneous ion-exchange membranes after thermal modification, Russ. J. Electrochem. 53 (2017) 398–410.
[62] N.P. Berezina, N.A. Kononenko, O.A. Dyomina, N.P. Gnusin, Characterization of ion exchange membrane materials: properties vs structure, Adv. Colloid Interface Sci. 139 (2008) 3–28.
[63] E.D. Belashova, N.A. Melnik, N.D. Pismenskaya, K.A. Shevtsova, A.V. Nebavsky, K.A. Lebedev, V.V. Nikonenko, Overlimiting mass transfer through cation-exchange membranes modified by Nafion film and carbon nanotubes, Electrochim. Acta 59 (2012) 412–423 .
[64] Y. Sedkaoui, A. Szymczyk, H. Lounici, O. Arous, A new lateral method for characterizing the electrical conductivity of ion-exchange membranes, J. Memb. Sci. 507 (2016) 34–42
[65] K.G. Sabbatovskii, A.I. Vilenskii, V.D. Sobolev, Electrosurface properties of poly(ethylene terephthalate) films irradiated by heavy ions and track membranes based on these films, Colloid J. 78 (2016) 573–575.
[66] K.A. Nebavskaya, V.V. Sarapulova, K.G. Sabbatovskiy, V.D. Sobolev, N.D. Pismenskaya, P. Sistat, M. Cretin, V.V. Nikonenko, Impact of ion exchange membrane surface charge and hydrophobicity on electroconvection at underlimiting and overlimiting currents, J. Membr. Sci. 523 (2017) 36–44
[67] E. Belova, G. Lopatkova, N. Pismenskaya, V. Nikonenko, C. Larchet, G. Pourcelly, The effect of anion-exchange membrane surface properties on mechanisms of overlimiting mass transfer, J. Phys. Chem. B. 110 (2006) 13458–13469.
[68] J.S. Newman, Electrochemical Systems, Prentice Hall, Englewood Cliffs, N.J, 1973.
[69] H.-W. Rösler, F. Maletzki, E. Staude, Ion transfer across electrodialysis membranes in the overlimiting current range: chronopotentiometric studies, J. Membr. Sci. 72 (1992) 171–179.
[70] N. Pismenskaya, N. Melnik, E. Nevakshenova, K. Nebavskaya, V. Nikonenko, Enhancing ion transfer in overlimiting electrodialysis of dilute solutions by modifying the surface of heterogeneous ion-exchange membranes, Int. J. Chem. Eng. 2012 (2012) 528290.
[71] S. Trasatti, O.A. Petrii, Real surface area measurements in electrochemistry, J. Electroanal. Chem., 327 (1992) 353–376.

[72] ISO 4287, Geometrical Product Specifications – Surface texture: Profile method – Terms, definitions and surface texture parameters, 1997.

[73] S. Suwal, C. Roblet, J. Amiot, L. Bazinet, Presence of free amino acids in protein hydrolysate during electroseparation of peptides: impact on system efficiency and membrane physicochemical properties, Sep. Purif. Technol. 147 (2015) 227–236.

[74] E.V. Krisilova, T.V. Eliseeva, G.Y. Oros, Estimation of effect of amino acid's sorption on surface state of ion-exchange membranes using atomic-force microscopy data, Prot. Met. Phys. Chem. Surf. 47 (2011) 39–42.

[75] S.A. Mareev, D.Yu. Butylskii, N.D. Pismenskaya, C. Larchet, L. Dammak, V.V. Nikonenko, Study of geometric heterogeneity of cmx cation-exchange membrane surface, Desalination, at print

[76] E. Güler , W. van Baak, M. Saakes, K. Nijmeijer, Monovalent-ion-selective membranes for reverse electrodialysis, J. Memb. Sci. 455 (2014) 254–270.

[77] P. Ribéreau-Gayon, Y. Glories, A. Maujean, D. Dubourdieu, Phenolic Compounds, in: Handb. Enol., John Wiley & Sons, Ltd, 2006, 141–203 pp.

[78] A.M. Simoes Costa, M.M. Costa Sobral, I. Delgadillo, A. Cerdeira, A. Rudnitskaya, Astringency quantification in wine: comparison of the electronictongue and FT-MIR spectroscopy, Sensor. Actuat. B-Chemical 207 (2015) 1095–1103.

[79] V. Sarapulova, E. Nevakshenova, N. Pismenskaya, L. Dammak, V. Nikonenko, Unusual concentration dependence of ion-exchange membrane conductivity in ampholyte-containing solutions: effect of ampholyte nature, J. Membr. Sci. 479 (2015) 28–38.

[80] S.D. Silva, R.P. Feliciano, L.V. Boas, M.R. Bronze, Application of FTIR-ATR to Moscatel dessert wines for prediction of total phenolic and flavonoid contents and antioxidant capacity, Food Chem. 150 (2014) 489–493.

[81] S.D. Silva, R.P. Feliciano, L.V. Boas, M.R. Bronze, Application of FTIR-ATR to Moscatel dessert wines for prediction of total phenolic and flavonoid contents and antioxidant capacity, Food Chem. 150 (2014) 489–493.

[82] G. Würdig, R. Woller, Chemie des Weines, Stuttgart: Eugen Ulmer GmbH, 1989.

[83] M. Moreno-Arribas, Wine chemistry and biochemistry, New York, Springer, 2009.

[84] J.-H. Choi, H.-J. Lee, S.-H. Moon, Effects of electrolytes on the transport phenomena in a cation-exchange membrane, J. Colloid Interface Sci. 238 (2001) 188–195.

[85] I. Rubinstein, B. Zaltzman, T. Pundik, Ion-exchange funneling in thin-film coating modification of heterogeneous electrodialysis membranes, Phys. Rev. E 65 (2002) 041507.

[86] R. Simons, Strong electric field effects on proton transfer between membrane-bound amines and water, Nature 280 (1979) 824–826.
[87] V.I. Zabolotskii, N.V. Shel'deshov, N.P. Gnusin, Dissociation of water molecules in systems with ion-exchange membranes, Russ. Chem. Rev. 57 (1988) 801.
[88] J.-H. Choi, S.-H. Moon, Structural change of ion-exchange membrane surfaces under high electric fields and its effects on membrane properties, J. Colloid Interface Sci. 265 (2003) 93–100.
[89] I. Rubinstein, B. Zaltzman, O. Kedem, Electric field effects in and around ion-exchange membranes, J. Membr. Sci. 125 (1997) 17–21.
[90] V.I. Zabolotsky, V.V. Nikonenko, N.D. Pismenskaya, On the role of gravitational convection in the transfer enhancement of salt ions in the course of dilute solution electrodialysis, J. Membr. Sci. 119 (1996) 171–181.
[91] E. Korzhova, N. Pismenskaya, D. Lopatin, O. Baranov, L. Dammak, V. Nikonenko, Effect of surface hydrophobization on chronopotentiometric behavior of an AMX anion-exchange membrane at overlimiting currents, J. Membr. Sci. 500 (2016) 161–170.
[92] M.A.K. Urtenov, E.V. Kirillova, N.M. Seidova, V.V. Nikonenko, Decoupling of the Nernst–Planck and Poisson equations. Application to a membrane system at overlimiting currents, J. Phys. Chem. B 111 (2007) 14208–14222.
[93] Yu.I. Kharkats, On the calculation of the rate constant of the charge transfer across the boundary of two dielectric media, Sov. Electrochem., 12 (1976) 1257–1263.
[94] V.V. Nikonenko, V.I. Vasil'eva, E.M. Akberova, A.M. Uzdenova, M.K. Urtenov, A.V. Kovalenko, N.P. Pismenskaya, S.A. Mareev, G. Pourcelly, Competition between diffusion and electroconvection at an ion-selective surface in intensive current regimes, Adv. Colloid Interface Sci. 235 (2016) 233-246.
[95] N.A. Mishchuk, Concentration polarization of interface and non-linear electrokinetic phenomena, Adv. Colloid Interface Sci. 160 (2010) 16–39.
[96] I. Rubinstein, B. Zaltzman, Equilibrium electroconvective instability, Phys. Rev. Lett. 114 (2015) 114502.
[97] I. Rubinstein, B. Zaltzman, Electro-osmotically induced convection at a permselective membrane, Phys. Rev. E Stat. Phys. Plasmas Fluids Relat. Interdiscip. Top. 62 (2000) 2238–2251.
[98] N.A. Mishchuk, S.S. Dukhin, Space-charge of a conducting particle in the over-limit current regime, Colloid J. USSR. 52 (1990) 427–431.

[99] H.-C. Chang, E. A. Demekhin, and V. S. Shelistov, Competition between Dukhin's and Rubinstein's electrokinetic modes, Phys. Rev. E. 86 (2012) 046319–9.
[100] I. Rubinstein, Electroconvection at an electrically inhomogeneous permselective interface, Phys. Fluids A 3 (1991) 2301–2309.
[101] N.A. Mishchuk, Electro-osmosis of the second kind near the heterogeneous ion-exchange membrane, in: Colloids Surfaces A Physicochem. Eng. Asp., 1998: pp. 75–89.
[102] S.S. Dukhin, Electrokinetic phenomena of the second kind and their applications, Adv. Colloid Interface Sci. 35 (1991) 173–196.
[103] V.V. Nikonenko, N.D. Pismenskaya, E.I. Volodina, Rate of generation of ions H+ and OH- at the ion-exchange membrane/dilute solution interface as a function of the current density, Rus. J. Electrochem. 41 (2005) 1205–1210.
[104] V.I. Zabolotsky, N.V. Sheldeshov, N.P. Gnusin, Dissociation of water molecules in systems with ion exchange membrane, Rus. Chem. Rev. 57 (1988) 1047–1049
[105] Park J.-S., Choi J.-H., Yeon K.-H., Moon S.-H. An approach to fouling characterization of an ion-exchange membrane using current–voltage relation and electrical impedance spectroscopy, J. Colloid Interface Sci. 294 (2006) 129–138
[106] Z. Slouka, S. Senapati, Y. Yan, H.-C. Chang, Charge inversion, water splitting, and vortex suppression due to DNA sorption on ion-selective membranes and their ion-current signatures, Langmuir 29 (2012) 8275–8283
[107] M.C. Martí-Calatayud, M. García-Gabaldón, V. Pérez-Herranz, Effect of the equilibria of multivalent metal sulfates on the transport through cation-exchange membranes at different current regimes, J. Membr. Sci. 443 (2013) 181–192
[108] M. Davidson, M. Wessling, A. Mani, On the dynamical regimes of pattern-accelerated electroconvection, Sci. Rep. 6 (2016) 22505.
[109] V.I. Zabolotsky, L. Novak, A.V. Kovalenko, V.V. Nikonenko, M.H. Urtenov, K.A. Lebedev, A.Y. But, Electroconvection in systems with heterogeneous ion-exchange membranes, Pet. Chem. 57 (2017) 779–789.